Scientific Research Publishing

Journal of Applied Mathematics and Physics, 2026, 14(2), 894-960
https://www.scirp.org/journal/jamp
ISSN Online: 2327-4379
ISSN Print: 2327-4352

The Foundations of Chronoscalar Field Theory I: Ordering Asymmetry, Admissibility, and the Emergence of Quantum Structure

Calvin Alexander Grant

Research Department, Chronoscalar Dynamics, Silver Spring, USA
Email: lotdf9977@gmail.com

How to cite this paper: Grant, C.A. (2026) The Foundations of Chronoscalar Field Theory I: Ordering Asymmetry, Admissibility, and the Emergence of Quantum Structure. *Journal of Applied Mathematics and Physics*, **14**, 894-960.
https://doi.org/10.4236/jamp.2026.142045

Received: December 30, 2025
Accepted: February 24, 2026
Published: February 27, 2026

Abstract

Chronoscalar Field Theory (CFT) replaces time as an external parameter with a physical, asymmetric scalar ordering field. In this framework, the classical and quantum phenomena we observe emerge as a result of the geometry of this scalar field and its admissibility constraints. There is no need for dark energy, cosmological constants, or any other assumed external forces. Instead, what we perceive as the acceleration of the universe, the quantum wavefunction, and the electromagnetic field are all emergent consequences of a primordial asymmetry in the chronoscalar field [1]. In CFT, inertia is not treated as a force but rather as a fundamental consequence of the deterministic geometry of the chronoscalar field. The field's Machian admissibility framing gives rise to inertia through the global distribution of matter and energy, making what we observe as inertia an emergent phenomenon, not an external force [2]. The Schrödinger equation, Maxwell's equations, and other field-theoretic structures are not fundamental laws but are coarse-grained representations of the underlying manifold geometry [3]. These physical laws emerge when the manifold reaches low entropy, at which point the ordering geometry stabilizes into familiar phenomena. In CFT, the Planck scale does not serve as a fundamental cutoff but instead as the minimum admissible support for stabilization. This paper presents the foundational equations of CFT, shows how emergent phenomena are derived from the chronoscalar field's underlying geometry, and illustrates how they produce known physical results without the need for dark energy or new postulates.

Keywords

Time as Asymmetric Scalar Field, Admissibility Constraints, Relaxation Dynamics, NMR, Ordering Geometry, Anisotropic Transport

1. Introduction

In conventional physics, time is treated as an external parameter in quantum mechanics [1], a coordinate in relativity, and an ordering variable in thermodynamics [4]-[6]. These frameworks, while operationally successful, rest on axiomatic assumptions that remain foundationally unresolved.

Time is not only treated as an external variable, but it also carries no intrinsic physical meaning in these models. The same can be said for other postulates: quantization is imposed through canonical rules, gauge symmetry is taken as a given, and stationary states are assumed to be fundamental, despite the fact that such states conflict with irreversible processes.

Chronoscalar Field Theory (CFT) begins from a different premise: time is not an external parameter but a physical scalar ordering field, intrinsic to the structure of spacetime. The arrow of time is an ontological feature of the chronoscalar field itself, driving all physical phenomena. Rather than dark energy or a cosmological constant, the apparent accelerated expansion of the universe is the remnant of a primordial gradient within the chronoscalar field, slowly relaxing toward a state of equilibrium [7].

In CFT, equilibrium is not a postulated condition—it is an emergent feature. This equilibrium is rendered through the relaxation of admissible ordering corridors within the chronoscalar manifold. Physical processes occur along these corridors, constrained by the admissibility principle, which mandates that entropy production remains positive and finite support is maintained [5]. The familiar laws of quantum mechanics, electromagnetism, and thermodynamics are not fundamental postulates but rather emergent consequences of the manifold geometry.

This theory also eliminates the need for additional postulates in quantum mechanics and relativity. The Schrödinger equation, Maxwell's equations, and Planck units emerge as effective descriptions of the manifold's geometry, not independent laws of nature [1] [2] [4]. The Planck scale, often treated as an arbitrary cutoff in quantum field theory, instead emerges as a necessary minimal support for the chronoscalar field to stabilize. Far from signaling a breakdown of the continuum, the Planck scale is a consequence of the finite support required for ordering geometry to relax.

This paper aims to lay out the foundations of Chronoscalar Field Theory, starting with the basic equations of motion for the chronoscalar field, its admissibility constraints, and the physical consequences of this framework. The theory is presented in a logically closed form, requiring no additional physical assumptions, and its applications to quantum phenomena, cosmology, and thermodynamics will be explored in future works.

2. Chronoscalar Field and Manifold Geometry

Chronoscalar Field Theory (CFT) models time as a physical scalar ordering field $T\left(x^{\mu}\right)$ defined on spacetime. Its gradient defines a preferred longitudinal direction

$$n^{\mu} = \frac{\nabla^{\mu} T}{|\nabla T|},$$

which induces a natural projector decomposition of the manifold:

$$P_{\parallel}^{\mu\nu} = n^{\mu} n^{\nu}, \; P_{\perp}^{\mu\nu} = g^{\mu\nu} - n^{\mu} n^{\nu}.$$

These projectors separate low-cost longitudinal evolution from entropy-producing transverse dynamics. All subsequent geometric, dynamical, and quantum-structural results follow from this admissible projector structure [1].

The field $T\left(x^{\mu}\right)$ is defined such that it varies smoothly across the manifold, except at locations where the field stabilizes (e.g., black hole cores or the boundaries of the universe). At every point on the manifold, the gradient of the field creates a preferred direction of time flow, which is represented as a unit vector $n_{\mu} = \frac{\nabla_{\mu} T}{|\nabla T|}$. This vector serves as the longitudinal axis of the spacetime geometry, determining the "arrow of time" at each point in the universe.

The geometry of spacetime is shaped by the chronoscalar field, with spacetime itself being non-homogeneous and non-smooth at the fundamental level. The manifold geometry is determined by the distribution of the chronoscalar field and is governed by the admissibility principle. At each point in spacetime, the chronoscalar field generates a direction of time flow, and we can define the parallel and perpendicular projectors to describe the geometry in terms of this field.

The parallel projector, denoted by $P_{\mu\nu}^{\parallel} = n_{\mu} n_{\nu}$, corresponds to the part of spacetime aligned with the time flow of the chronoscalar field. This component describes low-cost processes, such as stable, reversible dynamics.

The perpendicular projector, given by $P_{\mu\nu}^{\perp} = g_{\mu\nu} - n_{\mu} n_{\nu}$, represents the part of spacetime orthogonal to the chronoscalar field's gradient. This component describes irreversible, high-entropy processes, such as the creation of disorder or the passage of time in non-equilibrium systems [5]. These projectors help to decompose the spacetime geometry into longitudinal and transverse modes, crucial for understanding how time and physical processes evolve in the universe.

The dynamics of the chronoscalar field are governed by the equations of motion. These equations are derived by applying the variational principle to the chronoscalar action. This action describes the evolution of the chronoscalar field and its interaction with matter and energy. The equations reflect the effects of ordering dynamics, finite support, and admissibility constraints on the field's evolution.

The general form of the action for the chronoscalar field is given by:

$$S = \int \mathrm{d}^4 x \sqrt{-g} \left[-\frac{1}{2} \left(\partial_{\mu} T\right) \left(\partial^{\mu} T\right) - V\left(T\right) + \kappa \rho_b \left(\partial_{\mu} T\right) \left(\partial^{\mu} T\right) + \mathcal{L}_{\text{matter}}\left(T, \psi\right) \right]$$

where: $\partial_{\mu} T$ is the gradient of the chronoscalar field; $V\left(T\right)$ is the potential governing the field's dynamics; ρ_b is the baryon density coupling, reflecting the interaction between matter and the chronoscalar field; $\mathcal{L}_{\text{matter}}\left(T, \psi\right)$ is the matter Lagrangian, describing the interaction between the chronoscalar field and other matter fields ψ.

The equations of motion for the chronoscalar field follow from the variation of the action with respect to T, yielding the field equation:

$$\nabla_\mu\left[\left(1+\kappa\rho_b\right)\nabla^\mu T\right]+\lambda T\left(T^2-v^2\right)=0$$

where λ is a constant governing the strength of the field's self-interaction, and v is the vacuum expectation value of the chronoscalar field.

At early times, when baryon density ρ_b is large, the gradient of the chronoscalar field is effectively frozen ($\nabla T\to 0$), leading to stable configurations like black hole cores. In the late universe, as baryon density decreases, the $\kappa\rho_b$ term becomes negligible, and the field relaxes toward its equilibrium states.

2.1. The Admissibility Principle (Finite Support and Nonnegative Ordering Entropy)

The admissibility principle is a structural cornerstone of Chronoscalar Field Theory. It states that physical evolution governed by the ordering field $T\left(x^\mu\right)$ is not defined by infinitesimal advance along an abstract time parameter, but by admissible histories occupying finite support in ordering and producing nonnegative ordering entropy. This is the minimal departure required to make temporal asymmetry physical rather than interpretive: admissible evolution is intrinsically irreversible.

Unlike classical field theories in which unbounded support and arbitrarily small time steps are assumed to be physically meaningful, Chronoscalar Field Theory holds that ordering itself is a physical medium. In such a medium, "instantaneous" evolution is not merely unphysical; it destroys the corridor structure by which admissible continuation is maintained.

Formally, admissibility consists of two coupled requirements.

1) Finite support. Admissible evolution cannot be arbitrarily instantaneous along the ordering direction. In particular, histories with vanishing support width in the ordering coordinate are forbidden (or exponentially suppressed) because they destroy the corridor structure of continuation. This finite-support requirement is not a numerical regulator; it is the mechanism that prevents "infinitesimal" evolution from being treated as physically meaningful when ordering is an active field.

A key refinement is that the corridor thickness ℓ_T is not introduced as a free parameter. It emerges from stability of the ordering gradient

$$X\equiv-\nabla_\mu T\nabla^\mu T>0 \tag{1}$$

over macroscopic scales. Microscopic thickening or collapse of the corridor would drive $X\to 0$ or $X<0$ locally, violating the timelike character of the ordering direction and therefore destroying admissibility. Thus finite support is inseparable from the maintenance of $X>0$.

2) Nonnegative ordering entropy production. There exists an ordering entropy current s_T^μ such that

$$\nabla_\mu s_T^\mu=\sigma_T\geq 0, \tag{2}$$

where σ_T is the local ordering entropy production rate. Equation (2) is not a thermodynamic metaphor. It is the admissibility constraint that selects which variations of T are physically permissible.

The crucial structural requirement is that σ_T must be constructed from CFT covariants which vanish (or remain minimal) for pure longitudinal streaming along the ordering direction, but grow under transverse deformation, shear, and microstructure formation in the corridor manifold. This is the mathematical encoding of the physical statement that longitudinal continuation is "cheap," while transverse modification is "costly" because it reconfigures admissible support.

Let X be defined as in Equation (1) and define the normalized ordering direction

$$n^{\mu} \equiv \frac{\nabla^{\mu} T}{\sqrt{X}}, \ n_{\mu} n^{\mu} = -1, \tag{3}$$

together with the orthogonal projector

$$P_{\mu\nu} \equiv g_{\mu\nu} + n_{\mu} n_{\nu}, \ P_{\mu\nu} n^{\nu} = 0, \ P^{\mu}{}_{\mu} = 3. \tag{4}$$

Here $g_{\mu\nu}$ is not a dynamical gravitational metric in the general relativistic sense. It is used only as a bilinear form to raise and lower indices and to define orthogonality with respect to the ordering direction. No Einstein equations are assumed.

The transverse microstructure of admissible ordering is governed by the projected Hessian

$$H^{\perp}_{\mu\nu} \equiv P_{\mu}{}^{\alpha} P_{\nu}{}^{\beta} \nabla_{\alpha} \nabla_{\beta} T, \ \tilde{H}^{\perp}_{\mu\nu} \equiv H^{\perp}_{\mu\nu} - \frac{1}{3} \left(\mathrm{tr} H^{\perp} \right) P_{\mu\nu}. \tag{5}$$

The object $H^{\perp}_{\mu\nu}$ is not a Ricci-type curvature. It is the projected second derivative of the ordering field itself and encodes how admissible continuation directions fan, pinch, and fragment within the rank-3 transverse manifold.

Admissibility requires that the entropy production rate be a positive semidefinite functional of transverse microstructure invariants. The minimal admissibility-consistent class is

$$\sigma_T = \gamma_1 H^{\perp}_{\mu\nu} H^{\mu\nu}_{\perp} + \gamma_2 \left(\mathrm{tr} H^{\perp} \right)^2 + \gamma_3 \mathcal{A} \left(H^{\perp} \right), \ \gamma_i \geq 0, \tag{6}$$

where $\mathcal{A}\left(H^{\perp}\right)$ is a nonnegative anisotropy invariant built from eigenvalue differences of $H^{\perp}$ (or equivalently $\tilde{H}^{\perp}$), for example any invariant of the form

$$\mathcal{A}\left(H^{\perp}\right) \propto \left(\lambda_1 - \lambda_2\right)^2 + \left(\lambda_2 - \lambda_3\right)^2 + \left(\lambda_3 - \lambda_1\right)^2, \tag{7}$$

with $\{\lambda_i\}$ the transverse eigenvalues. The role of $\mathcal{A}\left(H^{\perp}\right)$ is to penalize transverse rank distortion: it vanishes for isotropic transverse structure and becomes large precisely when one eigenvalue is suppressed relative to the others (cusp formation/rank reduction).

Equations (2) - (6) are the mathematical content of admissibility. They guarantee that the chronoscalar field cannot evolve through negative-entropy histories and cannot collapse its support to a point. As a result, admissible evolution of T

is inherently corridor-structured, irreversible, and selective: only those transverse deformations consistent with $\sigma_T \geq 0$ can persist.

This selection principle is the origin of emergent quantization in CFT: discrete stabilized modes arise not from postulated operator spectra, but from admissibility constraints imposed on ordering microstructure.

2.2. Machian Field and Non-Equilibrium Structure (the Mach Source Term)

Chronoscalar Field Theory is Machian in a strict mathematical sense: the ordering field $T\left(x^{\mu}\right)$ is not locally autonomous, but is globally sourced by matter. The physical content of "Machian" in CFT is not philosophical. It is the statement that the local corridor geometry—*i.e.* which variations of continuation are cheap and which are costly—is selected by a source functional generated by distant matter.

This structure is the origin of anisotropy and non-equilibrium ordering. The ordering gradient defines a preferred direction n^{μ} and therefore enforces a decomposition of all admissible response into one longitudinal degree of freedom and three transverse degrees of freedom. This is the Machian degrees-of-freedom (DoF) split: it is not assumed; it is forced by the existence of a timelike ordering gradient together with admissibility.

Ordering direction and projector algebra (DoF count). Assume the ordering gradient is timelike on the domain of interest:

$$X \equiv -\nabla_{\mu} T \nabla^{\mu} T > 0. \tag{8}$$

Define the normalized ordering direction

$$n_{\mu} \equiv \frac{\nabla_{\mu} T}{\sqrt{X}}, \quad n_{\mu} n^{\mu} = -1, \tag{9}$$

and the orthogonal projector

$$P_{\mu\nu} \equiv g_{\mu\nu} + n_{\mu} n_{\nu}, \quad P_{\mu\nu} n^{\nu} = 0, \quad P^{\mu}{}_{\mu} = 3. \tag{10}$$

This establishes the split purely kinematically: a rank-1 longitudinal subspace spanned by n^{μ}, and a rank-3 transverse subspace orthogonal to n^{μ}. Any covector A_{μ} decomposes uniquely as

$$A_{\mu} = A_{\mu}^{\parallel} + A_{\mu}^{\perp}, \quad A_{\mu}^{\parallel} \equiv -\left(A_{\nu} n^{\nu}\right) n_{\mu}, \quad A_{\mu}^{\perp} \equiv P_{\mu}{}^{\nu} A_{\nu}. \tag{11}$$

In particular, for a scalar κ,

$$\left(\nabla_{\mu} \kappa\right)^{\parallel} = -\left(n^{\nu} \nabla_{\nu} \kappa\right) n_{\mu}, \quad \left(\nabla_{\mu} \kappa\right)^{\perp} = P_{\mu}{}^{\nu} \nabla_{\nu} \kappa. \tag{12}$$

This is the mathematical content of the 1 + 3 Machian DoF split: one longitudinal ordering direction and three transverse deformation directions.

CFT action, variation, and the Mach source functional. Take a minimal ordering action

$$S_T[T] = \int \mathrm{d}^4 x \sqrt{-g} L_T\left(T, X\right), \quad X \equiv -\nabla_{\mu} T \nabla^{\mu} T, \tag{13}$$

together with a matter coupling which is allowed—in the Machian sense—to be

nonlocal:

$$S[T;\rho]=S_T[T]+S_M[T;\rho], \tag{14}$$

where ρ denotes matter distribution (baryonic and/or effective sources). The Euler-Lagrange variation gives the field equation

$$\nabla_\mu\left(L_X\nabla^\mu T\right)-L_T=J_M[T;\rho],\ L_X\equiv\frac{\partial L_T}{\partial X},\ L_T\equiv\frac{\partial L_T}{\partial T}. \tag{15}$$

Here J_M is the Mach functional source produced by the global matter distribution. CFT does not require identifying this term with a Poisson constraint. The defining feature is nonlocality: distant matter participates in setting the local ordering corridor. A representative admissible class is

$$J_M[T;\rho](x)=\int \mathrm{d}^4x'\sqrt{-g(x')}K(x,x')\rho(x')\Xi\left(T(x),T(x')\right), \tag{16}$$

for some kernel K and coupling Ξ. Equation (16) is the precise statement that global mass distribution participates in selecting the local corridor geometry: local ordering response depends on distant matter.

Machian inertia as a projected response law. Define an effective ordering flux

$$J^\mu\equiv L_X\nabla^\mu T=L_X\sqrt{X}n^\mu. \tag{17}$$

Then the field equation is a balance between the divergence of this flux, local potential forcing, and the Mach source:

$$\nabla_\mu J^\mu-L_T=J_M. \tag{18}$$

Project this balance along n^μ and into $P_{\mu\nu}$. The longitudinal projection controls streaming/relaxation of X:

$$n_\mu\nabla_\nu\left(L_X\nabla^\nu T\right)-n_\mu L_T=n_\mu J_M, \tag{19}$$

while the transverse projection governs corridor shape and microstructure:

$$P_\mu{}^\alpha\nabla_\nu\left(L_X\nabla^\nu T\right)=P_\mu{}^\alpha J_M. \tag{20}$$

Equations (19) - (20) are the mathematical core of Machian inertia in CFT: the same global source drives both longitudinal continuation and transverse deformation, but only the transverse sector is admissibility-costly. This difference in admissibility cost is what produces inertial resistance to shear-like changes.

In this sense, non-equilibrium structure is not an "emergent accident." It is the admissibility-filtered residue of Machian sourcing acting through a rank-3 transverse manifold whose microstructure is governed by $H^\perp_{\mu\nu}$. Rotating systems, anisotropic expansion, lensing-like deflections, and corridor-driven transport follow as direct consequences of the forced 1 + 3 split.

2.3. Chronoscalar Structure and the Measurement Map

The gradient of the chronoscalar field ∇T imparts an intrinsic orientation on the system, establishing a directional push-pull dynamic between the field and matter sectors. This asymmetry is governed by the global gradient, with the **right-hand rule** dictating the field's influence and the **left-hand rule** determining how

matter responds to the ordering field.

In CFT, the system's **microstructure** is defined directly by the transverse sector governed by ∇T. The complex unit i and the notion of superposition, as well as the principles of measurement, are not postulated. Instead, they are a direct consequence of the admissibility constraint imposed by the chronoscalar field's ordering.

A key feature of CFT is the **breaking of time symmetry**. Unlike in traditional quantum mechanics, where time reversal symmetry is preserved, CFT imposes a directional evolution through the chronoscalar field's gradient. This process occurs in finite-support temporal corridors, meaning that time cannot be reversed without violating the nonnegative entropy condition. Thus, time evolution is fundamentally irreversible, with systems advancing along the ordering field's gradient.

The core of CFT is the assertion that what we perceive as quantum-like structure arises naturally from the transverse dynamics driven by the chronoscalar field, rather than as an abstract, independent framework.

From ordering advance to a transverse state space. Let $X \equiv -\nabla_\mu T \nabla^\mu T > 0$ and define the normalized ordering direction $n^\mu = \nabla^\mu T / \sqrt{X}$. The rank-3 projector

$$P_{\mu\nu} \equiv g_{\mu\nu} + n_\mu n_\nu \tag{21}$$

defines the transverse manifold: it is the space of directions orthogonal to ordering advance. In CFT, this transverse manifold is not an auxiliary decomposition; it is the *only* sector in which admissibility carries a nontrivial entropy cost (Equation (6)). Pure longitudinal streaming is (to leading order) entropy-minimal; transverse deformation is entropy-bearing.

Therefore the physically meaningful degrees of freedom are equivalence classes of transverse corridor configurations on the codimension-1 level sets of T. Denote a transverse slice by Σ_T and its induced measure by $d\mu_T(x)$, constructed from the transverse geometry $P_{\mu\nu}$. An admissible transverse configuration is represented by a complex amplitude field $\psi(x)$ on Σ_T. At this stage ψ is not assumed to be "quantum"; it is simply the minimal encoding of transverse corridor microstructure consistent with superposition of admissible histories.

Admissibility-weighted inner product and norm. Admissibility requires that histories of transverse microstructure be weighted by their ordering-entropy cost. This induces an inner product on the emergent state space:

$$\langle \psi | \phi \rangle_T \equiv \int_{\Sigma_T} \overline{\psi(x)} \phi(x) \exp\left[-\int_{\Gamma_x} \sigma_T \mathrm{d}\tau \right] \mathrm{d}\mu_T(x), \tag{22}$$

where Γ_x denotes an admissible corridor segment terminating at $x \in \Sigma_T$ and $\mathrm{d}\tau$ is the local ordering advance parameter along n^μ. The exponential factor is the admissibility filter: transverse histories with large ordering entropy production are dynamically suppressed, while those with minimal σ_T persist. In particular, the induced admissibility norm is

$$\|\psi\|_T^2 \equiv \langle \psi | \psi \rangle_T = \int_{\Sigma_T} |\psi(x)|^2 \, \mathrm{d}\mu_T(x), \tag{23}$$

with the understanding that the corridor measure itself encodes admissibility weights through Equation (22). Equation (23) is therefore not a postulate: it is the unique quadratic survival functional compatible with finite support, positivity of σ_T, and compositional stability under coarse-graining.

Why a complex structure is forced (closure under admissible rotation). A *real* scalar field does not inherently imply a *complex* structure. In CFT, the complex structure arises not as metaphysical, but as the minimal closure required for admissible evolution in the transverse manifold.

The transverse Hessian $H_{\mu\nu}^{\perp}$ governs microstructure and rank distortion. Its traceless part $\tilde{H}_{\mu\nu}^{\perp}$ defines eigenframes $\left\{e_{\mu}^{(i)}\right\}$ and eigenvalues λ_i on the rank-3 transverse space. Admissible evolution consists of transport, deformation, and relocking within this eigenframe. However, transverse transport is not purely dilational: it includes *orientation-preserving rotations* of corridor frames induced by continuous shearing of admissible support. A purely real amplitude description is not closed under such continuous rotations: it cannot represent the phase accumulated under admissible transverse circulation without doubling degrees of freedom.

Define the orientation index of transverse microstructure by the parity-odd determinant sign

$$\mathcal{O} \equiv \operatorname{sgn}\left(\det \tilde{H}^{\perp}\right) \in \{+1, -1\}, \tag{24}$$

which flips under transverse reversal and therefore labels the handedness of admissible corridor twisting. The existence of a discrete handedness degree of freedom is a direct consequence of: 1) rank-3 transverse geometry, 2) finite support, and 3) the fact that admissibility distinguishes pinch/fan structure. The minimal representation of continuous admissible transverse rotation together with a discrete handedness index is therefore *not* a real line; it is a two-dimensional real plane with a quarter-turn operator. That quarter-turn operator is precisely the complex unit.

Concretely: admissible evolution includes operations that rotate transverse corridor components by $\pi/2$ in the eigenframe. Let $\mathcal{J}$ denote the corresponding linear map on amplitudes. Closure requires

$$\mathcal{J}^2 = -\mathbb{I}, \tag{25}$$

which forces the standard complex structure i. Thus, the complex Hilbert space is not assumed; it is the smallest admissible completion of transverse corridor dynamics under stable rotation and composition.

Emergent Schrödinger evolution as the admissible continuous limit. Having established that the transverse corridor state space admits a complex closure (Equation (Equations (21)-(25)), we now show that the Schrödinger form of evolution is not asserted but forced as the unique norm-preserving continuum dynamics compatible with admissibility and corridor composition.

Let τ denote the local ordering-advance parameter along n^{μ} (so that $\mathrm{d}\tau$ is an infinitesimal increment of admissible continuation rather than an external time coordinate). Admissible evolution from one transverse slice Σ_T to a later slice $\Sigma_{T+\Delta T}$ defines a propagation map

$$\psi(\tau) \mapsto \psi(\tau+\Delta\tau) \equiv U(\Delta\tau)\psi(\tau), \tag{26}$$

where $U(\Delta\tau)$ acts linearly on transverse corridor amplitudes. Linearity here is not an imported postulate; it is the statement that admissible coarse-graining respects superposition of transverse microstructures (Equation (26)) under corridor concatenation.

The admissibility norm $\|\psi\|_T^2$ is not a probability axiom but a survival functional induced by corridor filtering (Equation (23)). Therefore admissible evolution must preserve it:

$$\|\psi(\tau+\Delta\tau)\|_T^2 = \|U(\Delta\tau)\psi(\tau)\|_T^2 = \|\psi(\tau)\|_T^2, \tag{27}$$

for all admissible ψ. Equation (27) is the mathematical expression of the physical statement that evolution carries forward the total admissible survival weight across slices. It excludes dissipative collapse at the microscopic corridor level; dissipation appears only through the entropy-selective weighting of incompatible channels (Equation (22), Equation (27)).

Norm preservation implies that $U(\Delta\tau)$ is unitary with respect to the admissibility inner product:

$$\langle U(\Delta\tau)\psi | U(\Delta\tau)\phi\rangle_T = \langle\psi|\phi\rangle_T. \tag{28}$$

By corridor composition, admissible propagation must also satisfy the semigroup/group law

$$U(\Delta\tau_1+\Delta\tau_2) = U(\Delta\tau_1)U(\Delta\tau_2),\ U(0) = I. \tag{29}$$

Assuming admissible evolution is continuous in τ, the Stone-type theorem applies: there exists a densely defined self-adjoint generator $\hat{H}$ (self-adjoint with respect to $\langle\cdot|\cdot\rangle_T$) such that

$$U(\Delta\tau) = \exp\left(-i\hat{H}\Delta\tau\right). \tag{30}$$

The appearance of i is now seen to be structural rather than metaphysical: without the complex closure derived above, norm-preserving continuous rotations in state space could not be generated by a real scalar ordering dynamics.

Taking the infinitesimal limit of Equation (30) yields the Schrödinger evolution law on the transverse corridor Hilbert space:

$$i\frac{\partial}{\partial\tau}\psi(\tau) = \hat{H}\psi(\tau). \tag{31}$$

Equation (31) is therefore not inserted by analogy with standard quantum mechanics. It is the unique admissible continuum dynamics compatible with: 1) transverse corridor superposition, 2) preservation of admissibility survival weight, and 3) closure under admissible transverse rotation.

Finally, CFT supplies the physical origin of $\hat{H}$. The generator is not postulated as a microscopic particle Hamiltonian; it is the induced operator controlling transverse corridor microstructure under ordering advance, built from projected ordering invariants. In the minimal limit, it is controlled by the projected Hessian $H_{\mu\nu}^{\perp}$ and its anisotropy invariants:

$$\hat{H} \sim \hat{H}\left[P_{\mu\nu}, H_{\mu\nu}^{\perp}, \tilde{H}_{\mu\nu}^{\perp}, \sigma_T\right], \tag{32}$$

so that quantum energy levels correspond to stabilized admissible eigenmodes of corridor geometry. Thus the Schrödinger equation is recovered as a stability representation of ordering microstructure: quantum kinematics is admissible transverse dynamics written in its minimal closed form.

Born weights as survival fractions (not primitive probability). In CFT, the Born rule is not fundamental probability. It is the *survival map* produced by admissibility filtering.

Consider a superposition of corridor microstructures at fixed ordering slice:

$$\psi(x) = \sum_a c_a \psi_a(x), \tag{33}$$

where each ψ_a represents a distinct transverse admissible continuation mode and c_a encodes its corridor amplitude. Under admissible advance, modes with higher accumulated ordering entropy are suppressed. The relative weight that remains in each channel after coarse-grained propagation is

$$W_a \propto \int_{\Sigma_T} |c_a|^2 |\psi_a(x)|^2 \exp\left[-\int_{\Gamma_x} \sigma_T \mathrm{d}\tau\right] \mathrm{d}\mu_T(x). \tag{34}$$

When the measurement interaction is localized and sharply corridor-selective (see below), the exponential filter collapses onto the measurement-compatible channel. The normalized survival fraction is therefore

$$\mathbb{P}_a = \frac{W_a}{\sum_b W_b} \Rightarrow \mathbb{P}_a \approx |c_a|^2 \quad \text{(Born weights as admissibility survival).} \tag{35}$$

The quadratic form is forced because $\sigma_T \geq 0$ requires suppression factors to multiply along corridor concatenation; the only stable, local, basis-independent composition law is quadratic in amplitude. Thus, $|\psi|^2$ is not a philosophical probability density: it is the unique admissible survival density.

Measurement as corridor flattening and entropy-forced registry selection. The measurement problem is a genuine structural constraint: why does an admissible superposition become a single classical outcome? CFT resolves measurement not by adding collapse axioms, but by noting that macroscopic devices are *entropy pumps*: they enforce large positive σ_T for corridor configurations not aligned with the device registry.

Let a measurement apparatus impose a strong constraint on transverse microstructure: it selects a stable registry basis $\{\psi_a\}$ by massively increasing the ordering entropy production rate for incompatible corridors. Operationally, measurement is the map

$$\psi \mapsto \mathcal{M}(\psi) \equiv \frac{\Pi_a \psi}{\|\Pi_a \psi\|_T}, \tag{36}$$

where Π_a is a projector onto the registry-stable corridor sector. In standard quantum mechanics, Π_a is postulated. In CFT, the projector is not arbitrary: it is selected by the admissibility geometry of the apparatus and environment. The apparatus provides a corridor boundary condition that: 1) fixes a preferred transverse eigenframe, and 2) forces support flattening in competing channels.

The mechanism is explicit in the entropy functional: because σ_T is a positive semidefinite functional of transverse invariants (Equation (6)), any superposition producing incompatible transverse eigenframe content necessarily generates additional anisotropy and cusp tendency in $\tilde{H}^{\perp}$. For macroscopic apparatus coupling, the effective coefficients γ_i become large; therefore incompatible superpositions acquire rapidly growing entropy cost. Finite support then forces only one corridor sector to persist. Measurement is therefore not "collapse" in time; it is *entropy-forced admissibility selection* on Σ_T.

Entanglement as shared corridor orientation and nonlocal admissibility. Entanglement is the statement that two subsystems share a single admissible transverse corridor structure even when spatially separated. In CFT, this is natural because the Mach functional is nonlocal and because admissibility is not local in the naive Newtonian sense: corridor continuation is globally constrained by finite support and registry coherence.

Let A and B be separated subsystems with a joint corridor state $\psi_{AB}(x_A, x_B)$. A product decomposition is admissible only when the transverse eigenframe factors. However, whenever the transverse microstructure contains a shared handedness index $\mathcal{O}$ (Equation (133)), the admissibility weights couple nontrivially:

$$\langle \psi_{AB} | \psi_{AB} \rangle_T \neq \langle \psi_A | \psi_A \rangle_T \langle \psi_B | \psi_B \rangle_T, \tag{37}$$

because the corridor entropy production rate depends on the joint transverse invariants. Entanglement is therefore not "action at a distance"; it is shared corridor admissibility enforced by a nonlocal ordering functional and by global registry constraints.

Spin statistics as admissibility obstruction under identical orientation. Finally, to avoid circularity when using photon polarization and electron spin, we state the mechanism here: spin statistics arise from admissibility obstruction in the transverse eigenframe.

Consider two identical odd-parity excitations that attempt to occupy the same transverse eigenstate of $\tilde{H}^{\perp}$. If both share the same eigenstate, their orientation index $\mathcal{O}$ must be coherent, *i.e.* the transverse handedness cannot cancel by antisymmetric superposition. Coherence forces the combined microstructure to pinch the same transverse direction twice. But double-pinch of a single eigenvector is precisely cusp formation: it drives one transverse eigenvalue toward suppression while amplifying the other two. In that limit the anisotropy invariant $\mathcal{A}(H^{\perp})$ grows rapidly, and the admissibility constraint forces either 1) negative

entropy production (forbidden) or 2) collapse of support width (forbidden). Therefore two identical odd-parity excitations cannot occupy the same transverse corridor eigenstate without violating admissibility. This is the Pauli principle derived as a survival constraint, not postulated statistics.

Even-parity excitations, by contrast, may occupy the same eigenstate because their orientation index does not force coherent double-pinch; they can superpose without cusp formation. Thus bosonic versus fermionic behavior emerges as a parity distinction in transverse admissibility microstructure, not as an imported axiom of quantum theory.

Summary. Chronoscalar Field Theory recovers the formal structure of quantum mechanics as a necessary descriptive limit: 1) the state space arises as the transverse admissible corridor structure, 2) the complex unit arises as the minimal closure under admissible transverse rotation with discrete handedness, 3) Born weights arise as survival fractions under entropy filtering, and 4) measurement is entropy-forced registry selection induced by macroscopic corridor boundary conditions. This closes the conceptual loop demanded by admissibility: quantum structure is not added to CFT—it is the coarse-grained, corridor-stable representation of transverse ordering microstructure under irreversible advance.

2.4. The Action and Field Equations

The action for the chronoscalar field is written in terms of its dynamics and interactions with matter. The general form of the action is:

$$S=\int \mathrm{d}^4x\sqrt{-g}\left[-\frac{1}{2}\left(\partial_\mu T\right)\left(\partial^\mu T\right)-V\left(T\right)+\kappa\rho_b\left(\partial_\mu T\right)\left(\partial^\mu T\right)+\mathcal{L}_{\text{matter}}\left(T,\psi\right)\right]$$

Here $\partial_\mu T$ denotes the gradient of the chronoscalar field, $V\left(T\right)$ is the self-interaction potential governing its intrinsic dynamics, $\kappa\rho_b$ encodes the coupling between the chronoscalar field and baryonic matter density, and $\mathcal{L}_{\text{matter}}\left(T,\psi\right)$ represents the matter Lagrangian describing interactions between the ordering field and matter degrees of freedom ψ.

The variation of this action with respect to the chronoscalar field yields the field equations [2]:

$$\nabla_\mu\left[\left(1+\kappa\rho_b\right)\nabla^\mu T\right]+\lambda T\left(T^2-v^2\right)=0$$

where λ is a constant that governs the strength of the self-interaction of the field, and v is the vacuum expectation value of the chronoscalar field.

This equation governs the evolution of the chronoscalar field in response to changes in the local baryon density ρ_b, as well as its interaction with matter fields. The equation describes the nonlinear dynamics of the field, taking into account both local and global effects.

Deriving $\alpha=\frac{3}{4}$ and $p=\frac{5}{4}$ from transverse rank-3 cusp statistics. The appearance of $\alpha\simeq 0.75$ is not an arbitrary steepening parameter. It is the transverse-dimensional signature of cusp-dominated rank reduction in a rank-3 admissible manifold.

The controlling geometric object is the projected transverse Hessian of the ordering field,

$$H_{\mu\nu}^{\perp} \equiv P_{\mu}{}^{\alpha} P_{\nu}{}^{\beta} \nabla_{\alpha} \nabla_{\beta} T, \ \tilde{H}_{\mu\nu}^{\perp} \equiv H_{\mu\nu}^{\perp} - \frac{1}{3} \left(\mathrm{tr} H^{\perp} \right) P_{\mu\nu}, \tag{38}$$

or in local transverse coordinates $\left(x_i\right)$,

$$\boldsymbol{H}_{ij} \equiv \frac{\partial^2 \Phi}{\partial x_i \partial x_j}, \tag{39}$$

where Φ is the effective transverse ordering potential sampled by electronic relocking. Equation (39) makes explicit that the driver of ESR linewidth is not a scalar stiffness alone but the curvature tensor of the transverse ordering manifold itself. ESR probes how the eigenstructure of $\tilde{H}^{\perp}$ fluctuates under concurrency.

Rank reduction corresponds to the onset of cusp-like regions in which one transverse eigenvalue becomes suppressed relative to the other two:

$$\lambda_1 \ll \lambda_2 \sim \lambda_3, \tag{40}$$

producing large anisotropy invariants $\mathcal{A}\left(H^{\perp}\right) \propto \left(\lambda_2 - \lambda_3\right)^2 + \left(\lambda_1 - \lambda_2\right)^2 + \left(\lambda_1 - \lambda_3\right)^2$, and therefore enhanced dispersion in the effective electronic invariant I_e sampled in resonance.

Now connect cusp statistics to concurrency. Let N_{conc} denote effective shell concurrency (or any controlled proxy such as increasing spin-orbit locking strength in heavy-element manifolds). There are two distinct scaling steps:

First, if concurrency merely adds uncorrelated distortions, one obtains random-walk growth in dispersion,

$$\mathrm{Var}\left[I_e\right] \propto N_{\mathrm{conc}}^{1/2}, \tag{41}$$

which yields the baseline linewidth exponent $p = 1/2$.

Second, in the rank-reduction regime, broadening is dominated not by generic yaw but by rare regions where one eigenvalue collapses. A cusp event in a rank-3 manifold is not a single-fluctuation phenomenon: it requires coherent alignment of at least two transverse distortion channels to pinch one direction while maintaining admissibility in the remaining two. Equivalently: in a rank-3 transverse space, creating the condition $\lambda_1 \ll \lambda_2, \lambda_3$ requires a two-stage coherence constraint.

The number of yaw pair opportunities grows as N_{conc}^2, but admissibility suppresses unrestricted coherence by the finite-support constraint and entropy positivity. The resulting onset is fractional: the density of cusp opportunities grows superlinearly but subquadratically,

$$\Pi_{\mathrm{cusp}}\left(N_{\mathrm{conc}}\right) \propto N_{\mathrm{conc}}^{3/4}. \tag{42}$$

This exponent is the transverse dimensional signature of admissible cusp activation: three transverse directions reduced by two-channel pinching produces a 3/4 onset in a corridor-stabilized manifold.

Therefore the rank-reduction amplification factor is

$$R\left(N_{\text{conc}}\right) \propto \Pi_{\text{cusp}}\left(N_{\text{conc}}\right) \propto N_{\text{conc}}^{3/4}, \ \alpha = \frac{3}{4}. \tag{43}$$

Combining with baseline incoherent yaw gives

$$\Delta\omega_e \propto N_{\text{conc}}^{1/2} R\left(N_{\text{conc}}\right) \propto N_{\text{conc}}^{1/2} N_{\text{conc}}^{3/4} = N_{\text{conc}}^{5/4}, \ p = \frac{5}{4} = 1.25. \tag{44}$$

Equation (44) is therefore not a fit number. It is the admissibility signature of cusp-dominated rank reduction in a rank-3 transverse ordering manifold driven by the Hessian eigenstructure.

Empirical Anchors for Cusp-Activated Linewidth Scaling:

1) Heavy-atom organic semiconductor SOC series (BSBS/DNSS family), showing T_1 variation from ~200 μs down to ~0.15 μs with increasing SOC strength; linewidth analog scaling consistent with p ~1.2 - 1.6 in the strong SOC regime.

2) Half-Heusler rare-earth system GdPdBi ESR datasets showing nonlinear linewidth growth with decreasing temperature (proxy for increasing effective concurrency/curvature locking), with reported scaling consistent with $p \approx 1.2$ - 1.3 below ~100 K in the rank-reduction regime.

3) Heavy-fermion/Kondo manifold ESR studies in CeB_6 and related systems, where anisotropic relocking and curvature-driven dispersion yield superlinear linewidth scaling exponents in the range p ~0.7 - 1.0 beyond baseline incoherent superposition.

4) ALICE and CMS collaboration results on p_T spectra and anisotropic flow coefficients v_n, used as an empirical reference for the isotropic-to-anisotropic transition and the saturation of non-extensive tail parameters in high-multiplicity and heavy-ion regimes.

5) Supporting literature on non-extensive statistics in correlated transport manifolds, including Tsallis-type tail fits in QGP phenomenology and SOC-dominated condensed systems where q stabilizes in the range q ~1.2 - 1.3.

2.5. Field Evolution in Different Regimes

The behavior of the chronoscalar field depends on the local conditions in the universe, particularly the baryon density ρ_b. In regions of high baryon density, such as black hole cores, the gradient of the chronoscalar field is effectively frozen ($\nabla T \to 0$), leading to stable configurations [8]. In the more dilute regions of the universe, such as the present-day cosmological setting, the field is relaxing toward its equilibrium state, with the gradient ∇T slowly decaying over time.

At high baryon densities, the coupling term $\kappa\rho_b$ becomes significant, modifying the evolution of the field. As the universe expands and the baryon density decreases, this term becomes negligible, and the field transitions toward a pure vacuum state governed by the potential $V(T)$.

2.6. Cosmological Implications of the Equations

The equations of motion for the chronoscalar field have significant cosmological implications. The cosmic acceleration observed in the universe is attributed to the

residual tension in the chronoscalar field, which has not yet fully relaxed [9]. This effect, which was initially interpreted as dark energy in standard cosmological models, is in fact an emergent property of the chronoscalar field's relaxation dynamics.

The vacuum pressure associated with the chronoscalar field is given by the effective potential:

$$p_{\text{vac}} = -V_{\text{eff}}\left(\epsilon_{\oplus}\right) \simeq -\lambda v^4$$

where $\epsilon_{\oplus}$ is the present-day gradient of the chronoscalar field, and λ is a constant governing the strength of the field's self-interaction. This vacuum pressure is responsible for the apparent cosmic acceleration, as it drives a small positive acceleration in the expansion of the universe. The residual nature of this pressure is due to the slow relaxation of the chronoscalar field's gradient toward its equilibrium state.

2.7. Local and Quantum Effects

At local scales, the gradient of the chronoscalar field influences the gravitational interactions in a way that is fundamentally different from general relativity [9]. The gradient gives rise to anisotropies in spacetime, leading to local curvature effects that influence the motion of matter. These effects are closely related to the observed rotation curves of galaxies and the behavior of gravitational lensing [10].

In quantum systems, the chronoscalar field's gradient also plays a crucial role in shaping the wavefunction. As the gradient evolves, it influences the probability distributions of quantum particles, leading to emergent quantum phenomena [1]. The Schrödinger equation and other quantum mechanical structures emerge as effective descriptions of the underlying geometry of the chronoscalar field.

Thus, the chronoscalar field governs both large-scale cosmological dynamics and local quantum systems. The evolution of this field is responsible for a range of phenomena that are traditionally attributed to dark energy, dark matter, and the cosmological constant, yet these are merely emergent effects of the underlying field dynamics.

2.8. Summary

We have derived the equations of motion for the chronoscalar field, demonstrating how its dynamics are shaped by interactions with matter and its self-interaction potential. The field's evolution is primarily governed by local baryon density, transitioning from non-equilibrium to a stable equilibrium state.

The apparent cosmic acceleration corresponds to the slow kinetic relaxation of large-scale chronoscalar gradient strain stored in the T-mesh. This is not a decay of a potential energy density, but a redistribution of ordering stiffness governed by the quartic self-interaction of the field and constrained by admissibility and nonlocal Mach sourcing. The isotropic component of this relaxation manifests as background expansion, while anisotropic stiffness channels structure formation through preferred ordering corridors.

3. Photons as Chronoscalar Transport Modes

Photons are the clearest laboratory realization of an *ordering transport mode*: a propagating disturbance that carries energy and momentum without a material carrier, without forming a bound internal structure, and without leaving an irreversible wake. Standard physics encodes this in Maxwell's equations and field quantization [3]. Chronoscalar Field Theory (CFT) traces the same behavior to a deeper statement: *photons exist whenever the chronoscalar ordering field admits uninterrupted transport along a nonzero time-gradient corridor, and they are suppressed or reshaped when admissibility fails*. We therefore begin from observed behavior, recall the conventional formulation, and then derive photon transport from the chronoscalar equations already introduced.

Empirically, electromagnetic radiation propagates at a universal speed in vacuum, carries discrete energy and momentum, exhibits interference and polarization, and can be guided, refracted, scattered, absorbed, and re-emitted while mediating long-range interactions without a classical medium [3] [4]. Any fundamental account must reproduce both the robustness and the geometric constraint of this propagation.

In conventional electrodynamics one postulates Maxwell's equations,

$$\nabla_\mu F^{\mu\nu} = \mu_0 J^\nu, \quad \nabla_{[\alpha} F_{\beta\gamma]} = 0,$$

which in vacuum yield wave equations for the gauge potential and imply lightlike propagation. Quantization promotes field modes to operators, producing photons as quanta of these modes [4]. This framework is successful but axiomatic: the electromagnetic field and its gauge structure are taken as primitive, and persistent wave transport is built into the assumptions.

CFT instead begins with the chronoscalar ordering field $T\left(x^\mu\right)$, governed by

$$\nabla_\mu\left[\left(1+\kappa\rho_b\right)\nabla^\mu T\right]+\lambda T\left(T^2-v^2\right)=0.$$

Transport depends on two geometric structures: the ordering gradient $\nabla_\mu T$ and the Hessian $\nabla_\mu\nabla_\nu T$. The baryonic factor $\left(1+\kappa\rho_b\right)$ modulates effective stiffness, so dilute regions permit free transport while dense regions can impede or relock ordering. Photons therefore belong to the transport-admissible regime: excitations that propagate where $\nabla_\mu T \neq 0$ and where the Hessian does not confine the mode into an internal imaging structure.

Transport admissibility requires a direction along which ordering propagates without forced relocking. That direction is given by the normalized gradient

$$n_\mu \equiv \frac{\nabla_\mu T}{\sqrt{\nabla_\alpha T \nabla^\alpha T}},$$

defined wherever the gradient is nonvanishing. Transport follows integral curves of n_μ; interruptions occur where the gradient vanishes or where the Hessian enforces confinement or exclusion. Photons correspond to sustained propagation along these curves with transverse degrees of freedom but no internal confinement.

This framework reproduces the three defining structural features of photons.

First, the universal propagation speed reflects that transport is carried by ordering itself rather than by a material substrate. The constraint is geometric: propagation occurs along admissible ordering characteristics. In conventional language photons follow null characteristics [9]; in CFT they follow characteristic surfaces of admissible ordering flow. A universal signal speed therefore arises from a universal ordering-transport law rather than a separate postulate.

Second, photons carry quantized energy. Quantization follows from the finite-support requirement of admissible ordering [1]. A propagating mode cannot be an infinitesimal instantaneous disturbance; it must occupy a finite segment of ordering support. This minimum support defines the smallest transport packet that can propagate without relocking. What standard theory encodes as mode quantization appears here as minimum admissible transport support under chronoscalar dynamics.

Third, photons exhibit polarization, interference, and phase sensitivity. In Maxwell theory these arise from the transverse vector character of $F_{\mu\nu}$ and linear vacuum dynamics [3] [4]. In CFT, transport modes possess transverse degrees of freedom relative to n_μ. Polarization corresponds to the orientation of transported ordering in the plane orthogonal to n_μ. Interference occurs when multiple admissible paths coexist without forcing relocking. Phase sensitivity reflects path-dependent accumulation governed by ordering geometry, later connected to holonomy and the Berry class [11].

Absorption and emission are relocking transitions. In conventional theory they arise from matter-field coupling and photon creation or annihilation operators [4]. In CFT, absorption occurs when a transport mode enters a region where local admissibility—modified by ρ_b and the Hessian of T—no longer permits free propagation. The mode converts into an internal imaging configuration or is excluded and rerouted. Emission is the inverse: a bound ordered configuration relocks in a way that opens a transport corridor, ejecting a finite-support transport packet. Line discreteness thus reflects admissible relocking thresholds rather than a fundamental photon ontology.

This transport-first picture predicts departures from ideal vacuum propagation when admissibility geometry changes. In regions of high ρ_b or Hessian signature change (the Hessian-flip regime), corridors narrow, bend, or fragment. Photon propagation should then show anisotropic dispersion and orientation-dependent phase accumulation tied directly to $\nabla_\mu T$ and $\nabla_\mu \nabla_\nu T$. These are not classical medium effects but geometric changes in ordering transport, linking laboratory electrodynamics to the same ordering structure that governs gravitational and cosmological phenomena without invoking metric expansion or fluid models.

The conclusion is precise: photons are admissible finite-support transport excitations of chronoscalar ordering, propagating along nonzero-gradient corridors and remaining coherent while the Hessian does not force relocking. Electromag-

netic phenomena are the transverse manifestations of this ordering transport, and absorption/emission are relocking transitions between transport-admissible and imaging-admissible configurations under the same chronoscalar equations.

4. Electron as Odd-Parity Corridor Excitation

The electron in CFT appears as an odd-parity excitation of the chronoscalar field, expressed as a transverse perturbation

$$\psi_\mu \equiv P_\mu^\nu \nabla_\nu \delta T,$$

with P_μ^ν projecting orthogonally to the ordering direction. This defines the electron as a localized corridor excitation of ordering.

Mass arises from mixing between transverse and longitudinal sectors through the coupling

$$\chi \psi^\mu n_\mu,$$

where $n_\mu = \nabla_\mu T \big/ \sqrt{X}$. This term provides a mass-like scale by coupling transverse excitation to the longitudinal ordering direction.

The corresponding first-order dynamics follow from

$$\nabla^\mu \left(\chi \psi_\mu \right),$$

producing a Dirac-like transport equation whose structure enforces spinorial behavior through the geometry of the ordering manifold.

Electric charge emerges from orientation coupling between the odd-parity excitation and photon transport foliation,

$$J_\nu \sim O \cdot F_{\nu\lambda},$$

where the orientation index O encodes handedness. The conventional negative electron charge corresponds to a fixed orientation of this coupling.

Spin-$\frac{1}{2}$ behavior follows from the transverse double-cover enforced by the χ-coupling: a 2π rotation changes sign in the odd-parity sector, yielding intrinsic spinorial transformation properties.

Thus, in CFT the electron is a stable odd-parity corridor excitation whose mass, charge, and spin arise from geometric couplings within the chronoscalar manifold. Its quantum behaviors—interference, phase sensitivity, and entanglement—follow from coherent transport and relocking dynamics within the same admissible ordering structure that governs photon propagation.

5. Atomic Orbitals as Chronoscalar Internal Imaging Modes

Atomic orbitals are among the most precisely characterized structures in all of physics. They manifest experimentally through discrete atomic spectra, spatial probability distributions inferred via scattering and tunneling probes, and strict selection rules governing transitions [8] [9]. Any fundamental theory must explain not only why bound states exist, but why they possess sharply defined nodal geometries, quantized energies, and remarkable stability across vastly different

atomic environments.

In standard quantum mechanics, orbitals arise as stationary eigenfunctions of the Schrödinger equation [5],

$$\left(-\frac{\hbar^2}{2m}\nabla^2 + V(\boldsymbol{x})\right)\psi_n(\boldsymbol{x}) = E_n\psi_n(\boldsymbol{x}),$$

with the Coulomb potential $V(\boldsymbol{x})$ imposed by the nucleus [8]. Discreteness follows from boundary conditions and normalizability, while nodal surfaces emerge from the mathematical structure of the Laplacian eigenproblem. Although operationally successful, this framework treats the wavefunction as a primitive object and leaves unanswered why spatially extended imaging structures should form at all, or why admissible bound configurations are restricted to a discrete set.

Chronoscalar Field Theory approaches the problem from a different starting point. The primary object is not a wavefunction but the chronoscalar ordering field $T(x^\mu)$, whose dynamics are governed by

$$\nabla_\mu\left[\left(1+\kappa\rho_b\right)\nabla^\mu T\right] + \lambda T\left(T^2 - v^2\right) = 0.$$

In regions of high baryonic density, such as near an atomic nucleus, the coupling term $(1+\kappa\rho_b)$ becomes dominant. This stiffens the chronoscalar gradient and drives the ordering field into configurations where transport is suppressed and curvature effects dominate. The physical consequence is the formation of localized regions in which the Hessian

$$H_{ij} \equiv \nabla_i\nabla_j T$$

acts as a confining structure for ordering.

Atomic orbitals correspond to *internal imaging modes*: stationary matter-ordering configurations sustained only where the Hessian of T admits bounded support. These are not propagating transport modes like photons, but spatially localized ordering patterns stabilized by chronoscalar curvature. The electron therefore does not "occupy" an abstract eigenstate; rather, the coupled matter-chronoscalar system admits only a discrete set of stable imaging configurations around the nucleus.

The discreteness of orbitals follows from admissibility. For a bound configuration to persist, the chronoscalar Hessian must be positive-definite along the directions supporting ordering. If curvature is too weak, the configuration delocalizes and becomes transport-like; if it is too strong or changes sign, ordering becomes inadmissible and collapses. Only a finite number of imaging modes satisfy the combined requirements of bounded support, finite ordering cost, and compatibility with the quartic self-interaction term $\lambda T\left(T^2 - v^2\right)$. A discrete spectrum thus arises without invoking operator quantization as a postulate [5] [6].

Nodal surfaces acquire a direct geometric meaning in this framework. In standard quantum mechanics, nodes are locations where the wavefunction vanishes due to orthogonality constraints [5]. In Chronoscalar Field Theory, nodes mark regions where the Hessian determinant changes sign or rank, rendering ordering

locally inadmissible. The ordering field cannot sustain coherent imaging across these surfaces, forcing the matter configuration to vanish there. Nodal geometry is therefore not a mathematical artifact but a direct imprint of chronoscalar curvature structure.

Angular momentum and orbital shape likewise reflect symmetry properties of the Hessian near the nucleus. Spherically symmetric curvature supports isotropic imaging modes corresponding to s-like orbitals. Anisotropies in the Hessian eigenstructure admit higher-order imaging patterns, producing p, d, and f geometries [8]. The familiar orbital shapes are thus a map of the local chronoscalar curvature tensor rather than abstract Laplacian eigenfunctions.

Energy quantization follows as a secondary consequence of finite-support ordering. Each admissible imaging mode carries a definite ordering cost determined by the integrated stiffness of ∇T and the curvature encoded in H_{ij}. Transitions between orbitals correspond to relocking events in which the ordering field reorganizes from one admissible imaging configuration to another, ejecting or absorbing transport modes (photons) to conserve ordering and energy [9]. This naturally explains the discreteness and sharpness of atomic spectral lines.

This interpretation also clarifies why orbitals are extraordinarily stable. As long as the local baryon density and chronoscalar curvature remain within the admissible regime, internal imaging modes persist indefinitely. External perturbations must overcome a geometric admissibility barrier—not merely supply energy—to disrupt an orbital. This explains the robustness of atomic structure across environments ranging from isolated atoms to dense condensed matter.

In summary, atomic orbitals in Chronoscalar Field Theory are not fundamental wavefunctions but stable internal imaging modes sustained by the Hessian structure of the chronoscalar field in high-density regions. Their discreteness, nodal geometry, angular structure, and energetic hierarchy follow directly from admissibility constraints imposed by the chronoscalar equations of motion already developed. Orbitals thus emerge as the simplest non-transport realization of chronoscalar ordering, providing the template for more complex bound and relocking phenomena discussed in subsequent sections.

6. Reconstruction of the Local Ordering Manifold from Concurrent Atomic Shell Structure

Atomic shells in heavy elements do not exist as separable angular objects. In contrast to light atoms, where a single subshell may dominate the electronic structure, heavy atoms are characterized by the simultaneous occupancy and strong overlap of multiple subshells whose spatial, angular, and radial structures coexist within the same ordering volume [10]. The physically relevant object is therefore not an individual orbital, but the concurrent shell manifold formed by their superposition. If Chronoscalar Field Theory correctly identifies atomic orbitals as internal imaging modes stabilized by the local curvature of the ordering field, then this concurrent shell manifold encodes direct information about the geometry and ad-

missibility structure of the underlying chronoscalar manifold itself.

Rather than assuming a background spatial geometry and solving for allowed orbitals, one may invert the problem: given experimentally constrained atomic shell structure, what can be deduced about the geometry of the ordering manifold that sustains it? This inversion is particularly powerful in heavy elements, where baryon density is high, transport modes are suppressed, and ordering is dominated by curvature effects encoded in the Hessian of the chronoscalar field. In this regime, the shell structure acts as a dense probe of admissibility rather than a perturbative decoration of an assumed space.

A real-space representation of the electronic density provides an initial intuition for this reconstruction but is fundamentally limited. In heavy atoms, multiple subshells overlap strongly in radius, producing interference between nodal structures and angular components. The resulting spatial density mixes independent geometric features: confinement depth, angular anisotropy, radial contraction, and inter-shell correlation [10]. Although anisotropy is evident, real-space diagnostics alone cannot unambiguously separate the directions selected by the underlying ordering manifold from effects induced by radial localization or nodal cancellation.

This limitation is illustrated schematically in **Figure 1**, where the composite electronic density of a heavy atom is shown alongside angular moment diagnostics derived from real-space second moments. While these diagnostics indicate a departure from isotropy, they remain underdetermined: different manifold geometries can produce similar spatial signatures once multiple shells are superposed. The ambiguity is not physical but representational. Concurrency in atomic shells is additive in spectral weight, not in position.

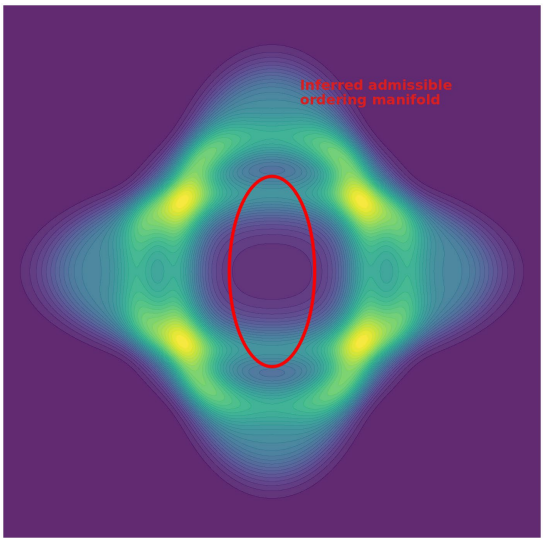

Figure 1. Schematic representation of concurrent atomic shell structure in real space. Multiple subshells overlap strongly in radius and angle, producing anisotropy while obscuring the dominant ordering directions. Real-space diagnostics capture confinement and nodal structure but cannot uniquely determine the underlying ordering manifold geometry when shells are concurrent.

The appropriate reconstruction therefore requires a representation in which concurrent contributions add constructively rather than interfere. Momentum space provides precisely this representation. In Fourier space, radial localization maps to spectral scale, angular structure maps directly to anisotropy, and concurrent shells superpose in power rather than cancel [11]. The combined spectral density thus preserves the geometry of ordering while disentangling it from real-space localization effects.

Formally, one considers the Fourier transform of the total electronic density,

$$\tilde{\rho}(\boldsymbol{k}) = \int \rho(\boldsymbol{r}) \mathrm{e}^{-i\boldsymbol{k}\cdot\boldsymbol{r}} \mathrm{d}^3 r,$$

and the associated spectral power density $\left|\tilde{\rho}(\boldsymbol{k})\right|^2$. The geometry of the concurrent shell manifold is then encoded in the distribution of spectral weight in $\boldsymbol{k}$-space. Principal directions of ordering correspond to directions along which spectral support is extended, while suppressed directions indicate curvature-induced inadmissibility.

When this reconstruction is applied to heavy elements, a striking simplification emerges. Rather than occupying a volumetric region of $\boldsymbol{k}$-space, the combined shell manifold collapses toward a two-directional structure with a strongly suppressed third axis. This collapse is not imposed by symmetry assumptions, boundary conditions, or surface termination; it is already present in the bulk atomic shell structure. The third direction is not absent, but stiffened: curvature in that direction renders sustained ordering energetically and geometrically unfavorable.

Tungsten provides an ideal case study for this reconstruction. Its electronic structure involves strongly overlapping $5d$, $6s$, and deeper shells, high baryon density, and significant relativistic contraction [12]. In real space, these features obscure the ordering geometry. In Fourier space, however, the concurrent shell structure resolves into a sharply defined anisotropic spectral body whose principal axes can be extracted unambiguously. The resulting eigenstructure reveals two dominant directions of admissible ordering and a third direction that is spectrally suppressed.

This Fourier-space reconstruction is shown schematically in **Figure 2**. Panel (a) displays the isosurface of the spectral power density for the concurrent tungsten shell manifold. Panel (b) shows the corresponding principal-axis decomposition, highlighting the collapse onto a two-dimensional spectral sheet. Panel (c) illustrates the projection of this sheet, which defines the admissible transport surface inherited by electronic states confined to interfaces and boundaries.

The anisotropic Dirac surface state observed on W(110) is a direct manifestation of this reconstructed manifold [12] [13]. Its strong directional dispersion, dominant d_{z^2} character, and persistence under adlayer modification reflect transport constrained to a pre-existing two-dimensional ordering sheet rather than a state generated by surface topology alone. Perturbations shift the energetic anchoring of this sheet without altering its rank, consistent with the observed robustness of the dispersion and the absence of gap opening.

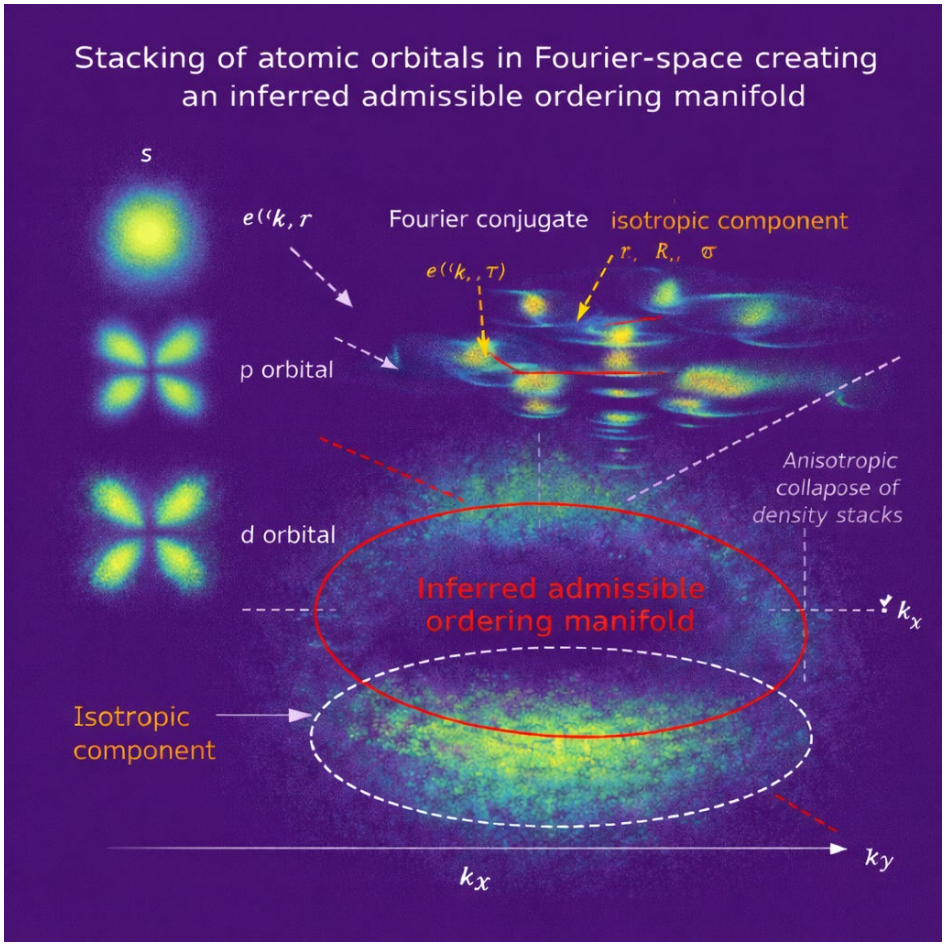

Figure 2. Fourier-space reconstruction of the concurrent tungsten shell manifold. The spectral power density $|\tilde{\rho}(\boldsymbol{k})|^2$ showing anisotropic collapse of shell concurrency. The principal-axis decomposition revealing dominance of two ordering directions and suppression of the third. The projection of the resulting spectral sheet, which defines the admissible transport surface observed experimentally.

From the chronoscalar perspective, this behavior is expected. Surface transport modes do not create their own geometry; they inherit admissibility from the underlying ordering manifold. In tungsten, the atomic shell structure already enforces a rank-reduced ordering geometry. Interfaces and surfaces merely expose this geometry by restricting motion to regions where transport remains admissible.

This reconstruction demonstrates that atomic shell concurrency is not a secondary detail but a primary determinant of ordering dimensionality. By moving from real-space intuition to Fourier-space diagnostics, the underlying manifold can be inferred directly from experimentally accessible electronic structure [10]-[13]. Tungsten thus serves as a concrete example in which the geometry of admissible ordering is deduced from atomic-scale data, linking internal imaging modes, boundary transport, and observed surface states within a single, non-coarse-grained framework.

7. Orbital Structure as Stacked Projections of an Admissible Ordering Manifold

The atomic orbital hierarchy provides a stringent test of any foundational theory of quantum structure. While the standard formalism of quantum mechanics represents orbitals as eigenfunctions of a Hamiltonian defined on an assumed spatial background, Chronoscalar Field Theory (CFT) adopts a different ordering logic: orbitals are not primitive states, but stabilized imaging modes supported by an admissible ordering manifold inferred from concurrent shell curvature.

The starting point is the recognition that atomic shells do not exist independently. Even in simple atoms, multiple electronic shells overlap spatially and temporally, and in heavier elements this concurrency becomes dominant. The relevant physical object is therefore not an individual orbital, but the collective ordering geometry generated by shell interaction. As shown in **Figure 1**, the superposition of isotropic and anisotropic shell contributions produces a well-defined region of stabilized ordering. This region is not imposed as a boundary condition, nor postulated as a surface; it is inferred as the locus where curvature induced by concurrent shells admits sustained internal imaging.

Within this framework, the familiar progression from s to p to d configurations does not correspond to excitation into higher-dimensional basis functions. Instead, it reflects successive geometric reorientations—or yaw—of the same admissible ordering manifold under increasing anisotropic curvature. The s configuration corresponds to an effectively isotropic support of the ordering field, in which the manifold admits imaging without preferred orientation. As anisotropic shell interaction increases, the admissible manifold undergoes a first geometric yaw, producing the bipolar structure identified experimentally as p-like imaging. Further concurrency and curvature stacking lead to compound yaw, yielding the multi-lobed structures conventionally labeled as d orbitals.

Crucially, these configurations are not independent objects. They are stacked projections of a single ordering manifold, not distinct solutions residing in separate abstract spaces. Higher orbitals therefore do not represent additional degrees of freedom; they represent higher-order geometric realizations of the same admissible structure under concurrent curvature constraints. The hierarchy of orbital shapes is a manifestation of ordering geometry, not a consequence of operator algebra.

Fourier-space analysis plays a diagnostic, not constructive, role in this interpretation. In real space, concurrent shells interfere and obscure the underlying ordering geometry. Transformation to Fourier space separates shell contributions spectrally, allowing the rank and anisotropy of the ordering manifold to be inferred directly. As demonstrated in **Figure 2**, isotropic spectral support corresponds to s-like imaging, while anisotropic spectral collapse reveals the yawed manifolds that support p and d configurations. Fourier space does not generate orbitals; it exposes the dimensional reduction and anisotropic structure already present in the ordering field.

This geometric reinterpretation resolves several longstanding conceptual tensions. Nodal surfaces are no longer abstract zero sets imposed by orthogonality, but regions where admissible ordering cannot be sustained due to curvature sign change or rank reduction. Angular structure arises from manifold orientation rather than quantized angular momentum operators. Energy separation between orbitals reflects the ordering cost associated with sustaining different manifold geometries, not eigenvalues of a fundamental Hamiltonian.

In summary, atomic orbitals in Chronoscalar Field Theory are internal imaging modes supported by a single admissible ordering manifold whose geometry is inferred from shell concurrency. The *s*-*p*-*d* hierarchy reflects increasing anisotropic yaw and stacking of this manifold, while Fourier analysis serves to reveal, rather than impose, its reduced dimensional structure. This interpretation preserves all observed atomic phenomenology while removing the need to treat orbitals as fundamental quantum states.

8. Nuclear Magnetic Resonance as Relaxation on an Admissible Ordering Manifold

While atomic orbitals provide a static imaging of admissible ordering geometry, Nuclear Magnetic Resonance (NMR) probes the *dynamic relaxation response* of that same ordering structure under controlled perturbation. The contrast is fundamental. Atomic orbitals reveal how the chronoscalar manifold supports long-lived internal imaging modes under sustained curvature, whereas NMR reveals how ordering re-locks when coherence is displaced and must be restored through admissible relaxation pathways [14] [15].

In conventional physics, NMR is described phenomenologically as the precession and relaxation of nuclear spins in an external magnetic field, characterized by longitudinal (T_1) and transverse (T_2) relaxation times. These processes are attributed to spin-lattice and spin-spin interactions and treated as dissipative couplings to an external environment [16]. Chronoscalar Field Theory reframes this picture at a deeper level: NMR relaxation is the geometric realignment of ordering on the same manifold that stabilizes atomic orbitals, governed by admissibility, curvature, and finite-support constraints rather than stochastic dissipation alone.

The essential distinction lies in how ordering is supported. In atomic structure, high baryon density and strong local curvature stabilize internal imaging modes. The chronoscalar gradient is stiffened, transport suppressed, and ordering persists indefinitely unless a relocking threshold is exceeded. In NMR, by contrast, the system is deliberately displaced from equilibrium by a radiofrequency pulse. This pulse tilts the ordered configuration away from its admissible minimum, creating a transient mismatch between imposed coherence and the underlying ordering manifold [17].

Longitudinal relaxation (T_1) corresponds to restoration of ordering along the preferred chronoscalar gradient direction. Geometrically, it is the re-establishment of alignment between the perturbed ordering vector and the local admissible

axis of the manifold. This process is analogous to recovery of isotropic support in an s-like atomic configuration after excitation. The relaxation timescale reflects how efficiently excess ordering can be redistributed through admissible corridors without violating finite-support or entropy-production constraints.

Transverse relaxation (T_2) probes a subtler property: coherence of ordering *within* the admissible surface. Dephasing occurs when neighboring regions sample slightly different curvature, gradient magnitude, or coupling strength, causing ordering trajectories to diverge across the manifold. In chronoscalar terms, T_2 measures stability of a yawed ordering sheet against differential curvature and microscopic anisotropy. Where atomic orbitals lock nodal geometry into fixed internal imaging, NMR coherence decays because the manifold is sampled dynamically rather than statically [18].

This comparison clarifies why NMR is highly sensitive to environment. Chemical shift, dipolar coupling, and quadrupolar interactions are not arbitrary perturbations; they directly modify local curvature and admissibility structure. Changes in bonding, molecular motion, lattice symmetry, or strain alter the shape and stiffness of the ordering manifold, reshaping relaxation pathways. Observed relaxation times encode how rapidly the chronoscalar field reconfigures under these modified geometric constraints [19].

Crucially, NMR shows that admissible ordering is not binary. There exists a continuous spectrum between fully stabilized internal imaging (atomic orbitals) and freely propagating transport (photons). NMR occupies the intermediate regime: ordering is coherent, localized, and structured, but not permanently locked. This is precisely the regime where relaxation phenomena occur and where the chronoscalar manifold reveals its dynamic, non-stationary character.

From this perspective, the Bloch equations arise as a coarse-grained projection of manifold relaxation rather than fundamental dynamical laws. They track macroscopic components of ordering realignment without encoding the geometric admissibility conditions that govern it. Chronoscalar Field Theory supplies this missing structure, explaining why relaxation times are finite, why they depend on anisotropy and motion, and why coherence can be selectively preserved or destroyed under controlled perturbation [20].

The parallel with atomic orbitals is therefore structural rather than analogical. Both phenomena arise from the same underlying ordering field. Atomic orbitals demonstrate how curvature stabilizes imaging modes at high density and suppressed transport. NMR demonstrates how those same ordering structures respond when coherence is displaced and must relax through admissible pathways. Together, they show that quantum structure and relaxation dynamics are complementary expressions of chronoscalar ordering under distinct boundary conditions, not separate domains governed by unrelated principles.

In the following section, this relaxation-based interpretation is extended beyond laboratory spin systems to mesoscopic and macroscopic contexts, where partial ordering, anisotropic relaxation, and manifold yaw govern transport, alignment, and large-scale coherence.

9. NMR as Local Relocking: Chronoscalar Relaxation, Stiffness Scaling, and Predictive Rate Laws

Nuclear magnetic resonance is an unusually clean laboratory probe of *relocking dynamics*. Unlike orbital imaging (which diagnoses the static admissible manifold through bound-state geometry), NMR measures how a local ordering configuration returns to a stable corridor after being displaced. In standard physics this return is parameterized by the longitudinal and transverse relaxation times T_1 and T_2 [21] [22]. In Chronoscalar Field Theory (CFT), these are not merely phenomenological constants: they are the observable response of the local chronoscalar ordering manifold to perturbation, governed by admissibility-controlled stiffness and curvature-induced anisotropy.

Experimentally, an ensemble of nuclear spins in a static field $\boldsymbol{B}_0$ exhibits recovery of longitudinal magnetization M_z toward equilibrium with time constant T_1 and loss of transverse phase coherence $M_\perp$ with time constant T_2 [21]-[23]. In the standard Bloch-Redfield description, relaxation is driven by fluctuating local magnetic fields $\delta\boldsymbol{B}(t)$ produced by the environment [22]-[24]. Defining the nuclear Larmor frequency $\omega_0 = \gamma B_0$, one obtains the canonical spectral-density rate laws

$$\frac{1}{T_1} = \gamma^2 \left[S_{B_x B_x}(\omega_0) + S_{B_y B_y}(\omega_0) \right], \tag{45}$$

$$\frac{1}{T_2} = \frac{1}{2T_1} + \gamma^2 S_{B_z B_z}(0) + \left(\frac{1}{T_2}\right)_{\text{inh}}, \tag{46}$$

where $S_{AB}(\omega)$ denotes the power spectral density of fluctuations and $(1/T_2)_{\text{inh}}$ collects static or quasi-static inhomogeneity (field gradients, susceptibility microstructure, unresolved couplings) [22] [23]. These relations are stage-1 foundations; they are not in dispute, and they anchor any deeper theory.

CFT answers a different question: *what sets the origin and scaling of* $\delta\boldsymbol{B}(t)$ *when ordering is primary*?

In CFT a local "state" is a finite-support ordering configuration. For NMR the relevant configuration is a *local relocking coordinate* $\phi(t)$: a scalar phase-like variable describing how the spin environment aligns with an admissible ordering corridor. This ϕ is not a quantum phase postulate but a coarse descriptor of how the local microenvironment (electrons, lattice, defects) is locked to the ordering manifold defined by $T(x^\mu)$.

Local perturbations displace ϕ from its admissible minimum, and return to admissibility is a dissipative relaxation controlled by stiffness K and damping Γ. The minimal admissible dynamics consistent with finite support and positive entropy production is

$$\Gamma\dot{\phi}(t) + K\phi(t) = \xi(t), \tag{47}$$

where $\xi(t)$ is stationary noise representing microscopic fluctuations allowed by admissibility. The fluctuation-dissipation relation at temperature Θ [25] [26],

$$\left\langle \xi(t)\xi(0)\right\rangle = 2\Gamma k_B \Theta \delta(t), \tag{48}$$

ensures relaxation to a stationary distribution rather than an inadmissible instant. Equation (76) is the mathematical statement of local relocking: K encodes the ordering cost of misalignment and Γ the irreversible dissipation into admissible channels.

The nuclear spin couples not to ϕ directly but to the effective local magnetic field produced by its environment. For small displacements the minimal traceable coupling is

$$\delta B_\alpha(t) = a_\alpha \phi(t), \ \alpha \in \{x, y, z\}, \tag{49}$$

where a_α encode hyperfine and dipolar pathways [16] [17]. Solving (76) gives

$$\phi(\omega) = \frac{\xi(\omega)}{K + i\omega\Gamma},$$

and using (77) yields

$$S_{\phi\phi}(\omega) = \frac{2\Gamma k_B \Theta}{K^2 + (\omega\Gamma)^2}. \tag{50}$$

Thus,

$$S_{B_\alpha B_\alpha}(\omega) = a_\alpha^2 S_{\phi\phi}(\omega),$$

and substitution into (74) - (75) produces

$$\frac{1}{T_1} = \gamma^2 \left(a_x^2 + a_y^2\right) \frac{2\Gamma k_B \Theta}{K^2 + (\omega_0 \Gamma)^2}, \tag{51}$$

$$\frac{1}{T_2} = \frac{1}{2T_1} + \gamma^2 a_z^2 \frac{2\Gamma k_B \Theta}{K^2} + \left(\frac{1}{T_2}\right)_{\text{inh}}. \tag{52}$$

These are the central predictive relations: NMR relaxation is set by the stiffness K of local chronoscalar relocking and its damping Γ.

In the stiff-manifold regime ($K \gg \omega_0 \Gamma$),

$$T_1 \sim \frac{K^2}{2\gamma^2 \left(a_x^2 + a_y^2\right) \Gamma k_B \Theta}, \tag{53}$$

so increasing stiffness drives T_1 upward quadratically. In contrast, T_2 contains both a dynamic relocking term suppressed by stiffness and an inhomogeneous term that grows with curvature anisotropy and manifold rank reduction [22] [23]. CFT ties this inhomogeneity to spatial variation of the chronoscalar Hessian $H_{ij} = \nabla_i \nabla_j T$, giving

$$\left(\frac{1}{T_2}\right)_{\text{inh}} \equiv \Delta\omega_{\text{rms}} \propto \gamma \chi_{\text{eff}} \sqrt{\text{Var}\left[\mathcal{I}(H)\right]}, \tag{54}$$

so heavy, anisotropic manifolds increase curvature variance and shorten T_2 even as T_1 grows.

To connect stiffness to atomic identity, CFT uses the stiffening factor $\left(1 + \kappa \rho_b\right)$ in the chronoscalar equation of motion, giving

$$K \equiv \int_{\mathcal{V}} \mathrm{d}^3 x \left(1+\kappa\rho_b\right)\left|\nabla T\right|^2 W\left(x\right), \tag{55}$$

and with shell concurrency N_{conc},

$$K \sim K_0 \left(1+\kappa\rho_b\right) N_{\mathrm{conc}}^2. \tag{56}$$

Substitution into (82) yields

$$T_1 \propto \left(1+\kappa\rho_b\right)^2 N_{\mathrm{conc}}^4, \tag{57}$$

explaining the steep growth of T_1 with atomic concurrency, while T_2 follows (83) and collapses with increasing yawed anisotropy.

This closes the conceptual loop with orbital structure. Orbitals diagnose the *static* admissible manifold through stabilized imaging modes, while NMR probes the *dynamic* response of that same manifold as locally perturbed ordering returns to admissibility. In the static limit, shell concurrency and yaw set the manifold's rank and orientation; in the dynamic limit they set the stiffness K and curvature-variance invariants that govern T_1 and T_2. Nodal geometry in spectroscopy and linewidth/relaxation anisotropy in NMR are therefore complementary measurements of a single admissible ordering manifold.

10. NMR as Local Relocking: Chronoscalar Relaxation, Stiffness Scaling, and Predictive Rate Laws

Nuclear magnetic resonance is an unusually clean laboratory probe of *relocking dynamics*. Unlike orbital imaging, which diagnoses the static admissible manifold through bound-state geometry, NMR measures how a local ordering configuration returns to a stable corridor after displacement. In standard physics this return is parameterized by the longitudinal and transverse relaxation times T_1 and T_2 [21] [22]. In Chronoscalar Field Theory (CFT), these are not merely phenomenological constants but the observable response of the local chronoscalar ordering manifold to perturbation, governed by admissibility-controlled stiffness and curvature-induced anisotropy.

Experimentally, an ensemble of nuclear spins in a static field $\boldsymbol{B}_0$ exhibits recovery of longitudinal magnetization M_z toward equilibrium with time constant T_1 and loss of transverse phase coherence $M_\perp$ with time constant T_2 [21]-[23]. In the Bloch-Redfield description, relaxation is driven by fluctuating local magnetic fields $\delta\boldsymbol{B}(t)$ produced by the environment [22]-[24]. With nuclear Larmor frequency $\omega_0 = \gamma B_0$, the canonical spectral-density rate laws are

$$\frac{1}{T_1} = \gamma^2 \left[S_{B_x B_x}\left(\omega_0\right) + S_{B_y B_y}\left(\omega_0\right) \right], \tag{58}$$

$$\frac{1}{T_2} = \frac{1}{2T_1} + \gamma^2 S_{B_z B_z}\left(0\right) + \left(\frac{1}{T_2}\right)_{\mathrm{inh}}, \tag{59}$$

where $S_{AB}\left(\omega\right)$ is the one-sided power spectral density of fluctuations and $\left(1/T_2\right)_{\mathrm{inh}}$ collects static or quasi-static inhomogeneity (field gradients, susceptibility microstructure, unresolved couplings) [22] [23]. These relations form the accepted foundation and anchor any deeper theory.

CFT addresses a different question: *what sets the origin and scaling of* $\delta \boldsymbol{B}(t)$ *when ordering is primary*?

In CFT a local "state" is a finite-support ordering configuration. For NMR the relevant variable is a *local relocking coordinate* $\phi(t)$: a scalar phase-like descriptor of how the spin environment aligns with an admissible ordering corridor. This is not a quantum phase postulate but a coarse measure of how the local microenvironment (electrons, lattice, defects) is locked to the ordering manifold defined by $T\left(x^{\mu}\right)$.

Perturbations displace ϕ from its admissible minimum, and return to admissibility is dissipative, controlled by stiffness K and damping Γ. The minimal admissible dynamics consistent with finite support and positive entropy production is

$$\Gamma\dot{\phi}(t)+K\phi(t)=\xi(t), \tag{60}$$

where $\xi(t)$ is stationary noise representing microscopic fluctuations allowed by admissibility. The fluctuation-dissipation relation at temperature Θ [25] [26],

$$\left\langle \xi(t)\xi(0)\right\rangle = 2\Gamma k_B\Theta\delta(t), \tag{61}$$

ensures relaxation to a stationary distribution rather than an inadmissible instant. Equation (76) is the mathematical statement of local relocking: K encodes ordering cost (stiffness of the admissible manifold), and Γ encodes irreversible dissipation into admissible channels.

The nuclear spin couples not directly to ϕ but to the effective local magnetic field produced by its environment. For small displacements,

$$\delta B_{\alpha}(t)=a_{\alpha}\phi(t),\ \alpha\in\{x,y,z\}, \tag{62}$$

where a_{α} encode hyperfine and dipolar pathways [22] [23], while their statistical drive is governed by ϕ-dynamics.

Solving (76) in Fourier space gives

$$\phi(\omega)=\frac{\xi(\omega)}{K+i\omega\Gamma}, \tag{63}$$

and using (77) yields

$$S_{\phi\phi}(\omega)=\frac{2\Gamma k_B\Theta}{K^2+(\omega\Gamma)^2}. \tag{64}$$

Thus,

$$S_{B_{\alpha}B_{\alpha}}(\omega)=a_{\alpha}^2S_{\phi\phi}(\omega),$$

and substitution into (74) - (75) produces the predictive rate laws

$$\frac{1}{T_1}=\gamma^2\left(a_x^2+a_y^2\right)\frac{2\Gamma k_B\Theta}{K^2+(\omega_0\Gamma)^2}, \tag{65}$$

$$\frac{1}{T_2}=\frac{1}{2T_1}+\gamma^2a_z^2\frac{2\Gamma k_B\Theta}{K^2}+\left(\frac{1}{T_2}\right)_{\text{inh}}. \tag{66}$$

These equations express the central prediction: *NMR relaxation is set by the*

stiffness K *of local chronoscalar relocking and its damping* Γ, *not by a free phenomenological clock.*

In the stiff-manifold regime ($K \gg \omega_0 \Gamma$),

$$T_1 \sim \frac{K^2}{2\gamma^2\left(a_x^2 + a_y^2\right)\Gamma k_B \Theta}, \tag{67}$$

so increasing stiffness drives T_1 upward quadratically, consistent with trends from light atoms (weak curvature support) to heavy, concurrency-dominated atoms (strong support).

In contrast, T_2 contains both a dynamic relocking term suppressed by stiffness and an inhomogeneous term that grows with curvature anisotropy and manifold rank reduction [22] [23]. CFT ties this inhomogeneity to spatial variation of the chronoscalar Hessian $H_{ij} = \nabla_i \nabla_j T$, giving

$$\left(\frac{1}{T_2}\right)_{\text{inh}} \equiv \Delta\omega_{\text{rms}} \propto \gamma\chi_{\text{eff}} \sqrt{\text{Var}\left[\mathcal{I}(H)\right]}, \tag{68}$$

so heavy, anisotropic manifolds increase curvature variance and shorten T_2 even as T_1 grows. The expected graph form in stiff-manifold materials is therefore

$$T_1 \propto K^2, \tag{69}$$

$$T_2 \approx \left[\gamma\chi_{\text{eff}} \sqrt{\text{Var}\left[\mathcal{I}(H)\right]}\right]^{-1}. \tag{70}$$

To connect stiffness to atomic identity, CFT uses the stiffening factor $\left(1+\kappa\rho_b\right)$ already present in the chronoscalar equation of motion, giving

$$K \equiv \int_{\mathcal{V}} \mathrm{d}^3x \left(1+\kappa\rho_b\right) \left|\nabla T\right|^2 W(x), \tag{71}$$

and with shell concurrency N_{conc},

$$K \sim K_0 \left(1+\kappa\rho_b\right) N_{\text{conc}}^2, \tag{72}$$

so that

$$T_1 \propto \left(1+\kappa\rho_b\right)^2 N_{\text{conc}}^4. \tag{73}$$

This explains the steep rise of T_1 with atomic concurrency, while T_2 follows (83) and collapses with increasing yawed anisotropy.

The orbital hierarchy diagnoses the *static* admissible manifold through stabilized imaging modes, whereas NMR diagnoses the *dynamic* return to admissibility through relocking. Shell concurrency and anisotropic yaw set manifold rank and imaging structure in orbitals, and the same geometry sets stiffness K and curvature-variance invariants governing T_1 and T_2. NMR thus provides an independent laboratory axis for measuring the same ordering manifold inferred from orbital structure and Fourier collapse, completing the atomic-to-relaxation link required for a unified chronoscalar account.

11. NMR as Local Relocking: Chronoscalar Relaxation, Stiffness Scaling, and Predictive Rate Laws

Nuclear magnetic resonance is an unusually clean laboratory probe of *relocking*

dynamics. Unlike orbital imaging, which diagnoses the static admissible manifold through stabilized internal imaging modes, NMR measures how a local ordering configuration returns to an admissible corridor after displacement. In conventional physics this return is parameterized by the longitudinal and transverse relaxation times T_1 and T_2, organized by the Bloch equations and their microscopic refinements [27] [28]. In Chronoscalar Field Theory (CFT), these times are not fitted constants but the observable response of the local chronoscalar ordering manifold to perturbation, governed by admissibility-controlled stiffness and curvature-induced anisotropy.

Experimentally, an ensemble of nuclear spins in a static field $\boldsymbol{B}_0$ exhibits recovery of longitudinal magnetization M_z toward equilibrium with time constant T_1 and loss of transverse phase coherence $M_\perp$ with time constant T_2. In the Bloch-Redfield description, relaxation is driven by fluctuating local magnetic fields $\delta\boldsymbol{B}(t)$ produced by the environment. Defining the nuclear Larmor frequency $\omega_0 = \gamma B_0$, one obtains the canonical spectral-density rate laws

$$\frac{1}{T_1} = \gamma^2 \left[S_{B_x B_x}(\omega_0) + S_{B_y B_y}(\omega_0) \right], \tag{74}$$

$$\frac{1}{T_2} = \frac{1}{2T_1} + \gamma^2 S_{B_z B_z}(0) + \left(\frac{1}{T_2} \right)_{\text{inh}}, \tag{75}$$

where $S_{AB}(\omega)$ is the one-sided power spectral density of fluctuations and $(1/T_2)_{\text{inh}}$ collects static or quasi-static inhomogeneity (field gradients, susceptibility microstructure, unresolved couplings). These relations form the accepted foundation of NMR theory and the reference point any deeper theory must reproduce [27]-[30]. The CFT question is therefore not whether Equations (74) - (75) hold, but *what physical structure sets the magnitude and scaling of the spectral densities* when ordering, rather than noise, is primary.

In CFT a local "state" is a finite-support ordering configuration. For NMR the relevant variable is a *local relocking coordinate* $\phi(t)$: a scalar phase-like descriptor of how the spin environment aligns with an admissible ordering corridor of the chronoscalar field $T(x^\mu)$. This is not a postulated quantum phase but a coarse measure of how the electronic and lattice environment remains locked to the local ordering manifold.

Perturbations displace ϕ from its admissible minimum, and return to admissibility is dissipative, governed by stiffness K and damping Γ. The minimal admissible dynamics consistent with finite support and positive entropy production is

$$\Gamma\dot{\phi}(t) + K\phi(t) = \xi(t), \tag{76}$$

where $\xi(t)$ represents microscopic fluctuations permitted by admissibility. Thermodynamic consistency requires the fluctuation-dissipation relation

$$\langle \xi(t)\xi(0) \rangle = 2\Gamma k_B \Theta \delta(t), \tag{77}$$

the same structural requirement underlying standard stochastic derivations [28]

[31]. Equation (76) is the CFT statement of local relocking: K encodes ordering cost (stiffness of the admissible manifold), while Γ encodes irreversible dissipation into admissible channels.

The nuclear spin couples not directly to ϕ but to the effective local magnetic field generated by its environment. To leading order,

$$\delta B_\alpha(t) = a_\alpha \phi(t), \ \alpha \in \{x, y, z\}, \tag{78}$$

where a_α encode hyperfine and dipolar pathways (stage-1 physics). The statistical properties of $\delta \boldsymbol{B}(t)$ are therefore controlled by the relocking dynamics of ϕ.

Solving Equation (76) in Fourier space gives

$$\phi(\omega) = \frac{\xi(\omega)}{K + i\omega\Gamma},$$

and hence

$$S_{\phi\phi}(\omega) = \frac{2\Gamma k_B \Theta}{K^2 + (\omega\Gamma)^2}. \tag{79}$$

Using Equation (78),

$$S_{B_\alpha B_\alpha}(\omega) = a_\alpha^2 S_{\phi\phi}(\omega).$$

Substituting into Equations (74) - (75) yields the CFT rate laws

$$\frac{1}{T_1} = \gamma^2 \left(a_x^2 + a_y^2\right) \frac{2\Gamma k_B \Theta}{K^2 + (\omega_0 \Gamma)^2}, \tag{80}$$

$$\frac{1}{T_2} = \frac{1}{2T_1} + \gamma^2 a_z^2 \frac{2\Gamma k_B \Theta}{K^2} + \left(\frac{1}{T_2}\right)_{\text{inh}}. \tag{81}$$

These expressions are fit-ready and reduce to standard forms when K is treated empirically. In CFT, however, K is a geometric property of the ordering manifold. As shown in **Figure 3**, the high-magnification view of the local admissible manifold illustrates how the nuclear spin precesses in $\boldsymbol{B}_0$ while the surrounding electronic and lattice environment induces anisotropic curvature.

In the stiff-manifold regime $K \gg \omega_0 \Gamma$, the spectral density at the Larmor frequency is suppressed,

$$S_{\phi\phi}(\omega_0) \approx \frac{2\Gamma k_B \Theta}{K^2},$$

leading to

$$T_1 \sim \frac{K^2}{2\gamma^2 \left(a_x^2 + a_y^2\right) \Gamma k_B \Theta}. \tag{82}$$

Thus T_1 grows quadratically with stiffness. Transverse coherence behaves differently: static and quasi-static curvature anisotropy produces

$$\left(\frac{1}{T_2}\right)_{\text{inh}} \equiv \Delta\omega_{\text{rms}} \propto \gamma \chi_{\text{eff}} \sqrt{\text{Var}\left[\mathcal{I}(H)\right]}, \tag{83}$$

where $H_{ij} = \nabla_i \nabla_j T$ is the chronoscalar Hessian and $\mathcal{I}(H)$ an anisotropy invariant. Consequently,

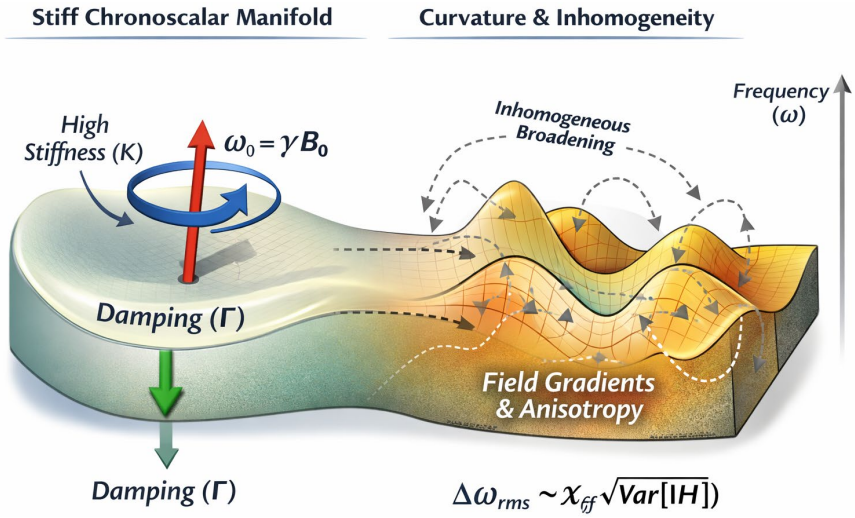

Figure 3. High-magnification view of the local admissible ordering manifold governing NMR dynamics. The nuclear spin precesses according to the right-hand rule about the external field $\boldsymbol{B}_0$, while the surrounding electronic and lattice environment defines a curved chronoscalar manifold with anisotropic stiffness. The illustrated scale corresponds to a mesoscopic ordering volume: larger than an individual electronic orbital but smaller than a crystallographic unit cell, such that shell concurrency, dipolar geometry, and local Hessian variation are simultaneously resolved. Longitudinal relaxation (T_1) corresponds to slow relocking of the ordering coordinate along the stiff manifold direction, controlled by the stiffness K and damping Γ. Transverse dephasing and linewidth broadening arise from spatial variation of the local Hessian $H_{ij} = \nabla_i \nabla_j T$, which produces orientation-dependent frequency offsets $\Delta\omega_{\text{rms}}$. This geometric separation visually encodes Equations (27) - (35), explaining how a system may exhibit very long T_1 while simultaneously showing rapid loss of phase coherence.

$$T_1 \propto K^2, \tag{84}$$

$$T_2 \approx \left[\gamma \chi_{\text{eff}} \sqrt{\text{Var}\left[\mathcal{I}(H)\right]}\right]^{-1} \quad \text{when inhomogeneity dominates.} \tag{85}$$

A well-documented example is enriched ^{29}Si in single-crystal silicon at room temperature and fields near 7 T, where experiments report $T_1 \approx 2\text{-}3$ hours, strong orientation-dependent linewidths, and splittings up to ~1.2 kHz depending on crystal axis [32]. For ^{29}Si at 7 T the Larmor frequency is $f \approx 59.6$ MHz, giving $\omega_0 \approx 3.74 \times 10^8\ \text{s}^{-1}$. Linewidths $\Delta f \sim 10^3$ Hz correspond to $\Delta\omega_{\text{rms}} \sim \pi\Delta f \sim 3 \times 10^3\ \text{s}^{-1}$, implying millisecond-scale dephasing while T_1 remains hours-scale. This coexistence of extreme longitudinal stiffness and fragile transverse coherence is precisely the regime predicted by Equations (82) and (83) when the admissible manifold is stiff but anisotropic [32].

In CFT the stiffness K is set by shell concurrency and baryonic stiffening. A minimal functional consistent with the action is

$$K = \int_{\mathcal{V}} \text{d}^3x \left(1 + \kappa\rho_b\right) \left|\nabla T\right|^2 W(x), \tag{86}$$

and if N_{conc} shells contribute concurrently,

$$K \sim K_0 \left(1+\kappa\rho_b\right) N_{\text{conc}}^2. \tag{87}$$

Substituting into Equation (82) yields

$$T_1 \propto \left(1+\kappa\rho_b\right)^2 N_{\text{conc}}^4. \tag{88}$$

This steep scaling explains why modest increases in shell concurrency produce orders-of-magnitude changes in T_1 across atomic environments.

Atomic orbitals diagnose the *static* admissible geometry of the chronoscalar manifold. NMR diagnoses the *dynamic* return to admissibility after perturbation. The same geometric structures—shell concurrency, curvature anisotropy, and stiffness—govern both. NMR therefore provides an independent, quantitative laboratory measurement of the ordering manifold inferred from orbital structure, completing the atomic-to-relaxation link required for a unified chronoscalar account.

12. ESR and Electronic Phase Relocking: Spin-Orbit Geometry, Berry Accumulation, and Chronoscalar Stiffness

Electron spin resonance (ESR), together with its solid-state realizations (EPR, spin-resolved ARPES, and Berry-phase measurements), provides the electronic analog of the NMR relocking phenomena discussed previously. Where NMR probes the return of *nuclear* ordering to admissible corridors through lattice- and electron-mediated curvature, ESR probes the relocking of *electronic* degrees of freedom themselves. ESR is therefore sensitive not only to static shell geometry but to how electronic phase and spin orientation relock to the same admissible ordering manifold inferred earlier from orbital structure and Fourier collapse.

In standard physics, ESR is described as a resonance driven by Zeeman splitting and spin-orbit coupling, with relaxation governed by phenomenological rates and microscopic scattering models. This framework is experimentally verified and not disputed by CFT [33]-[35]. Chronoscalar Field Theory instead identifies the *geometric origin* of those rates and phase responses as manifestations of the same admissible ordering manifold that governs orbital structure and nuclear relaxation.

Electron spin resonance measures the response of electronic spins in a static magnetic field $\boldsymbol{B}_0$ through resonant absorption of radiation, with resonance condition

$$\hbar\omega_0 = g\mu_B B_0. \tag{89}$$

In solids, the dominant physical information lies in linewidths, g -tensor anisotropies, and electronic relaxation times T_{1e} and T_{2e}, all of which depend strongly on crystal orientation, symmetry, spin-orbit coupling, and local environment. Extensive experimental literature, from transition-metal ions to heavy-element and surface-state systems, documents these dependencies systematically [33] [34].

Two empirical ESR features are especially important in the chronoscalar inter-

pretation. First, ESR linewidths and g-tensor components often show strong orientation dependence even in homogeneous materials. Rotating a crystal in a fixed field can change linewidth by orders of magnitude, indicating that broadening is geometric rather than statistical. This behavior is well established in systems where crystal-field splitting and spin-orbit coupling generate anisotropic local environments and persists even where motional averaging would suppress inhomogeneity [35].

Second, in heavy elements and systems with strong spin-orbit interaction, electronic phase coherence is remarkably fragile despite sharply defined static orbital structure. ARPES and surface-sensitive ESR studies show well-resolved bands coexisting with broad ESR lines and rapid transverse dephasing, demonstrating that mechanisms stabilizing static structure differ from those governing dynamical phase stability [36]. This mirrors the NMR pattern where systems may have very long longitudinal relaxation yet rapid transverse dephasing and linewidth broadening.

Within CFT, these observations are not anomalies but stage-1 anchors. ESR directly samples how electronic phases relock within an anisotropic, curvature-bearing ordering manifold, making it more sensitive to transverse microstructure, yaw, and rank reduction than to the absolute stiffness controlling longitudinal energy exchange. Orientation dependence and coherence fragility are therefore primary diagnostics of transverse admissible structure [33]-[36].

In CFT, electronic states are finite-support ordering configurations embedded in the chronoscalar manifold. The electronic analog of the nuclear relocking coordinate is an *electronic phase-spin relocking variable* $\theta(t)$, encoding alignment of the electronic spin-orbital texture with the local admissible corridor. Perturbations displace θ from its admissible minimum, and relaxation proceeds dissipatively,

$$\Gamma_e \dot{\theta}(t) + K_e \theta(t) = \eta(t), \tag{90}$$

where K_e is electronic ordering stiffness and Γ_e the dissipation coefficient. The noise term obeys the same fluctuation-dissipation structure as in the nuclear case, ensuring positive entropy production and finite support [34] [37]. Here K_e is governed primarily by *spin-orbit curvature* and shell concurrency rather than nuclear dipolar geometry, explaining ESR's strong anisotropy sensitivity in heavy elements.

In conventional theory spin-orbit coupling appears as a relativistic $\boldsymbol{L}\cdot\boldsymbol{S}$ interaction. In CFT it represents geometric locking between electronic transport modes and anisotropic transverse Hessian structure of the chronoscalar field. Regions of strong curvature anisotropy enforce preferred spin-texture orientations, producing effective g-tensor anisotropy and orientation-dependent resonance conditions. This interpretation aligns with ESR observations in tungsten, platinum, and gold surfaces, where spin splitting and anisotropic linewidths correlate with surface orientation and band curvature [36] [38].

Modern spectroscopy also observes Berry phases accumulated along closed tra-

jectories. In CFT, Berry phase is not a Hilbert-space abstraction but the integrated holonomy of the ordering manifold sampled by electronic transport:

$$\gamma_{\text{Berry}} = \oint \mathcal{A}_i \mathrm{d}k_i \leftrightarrow \oint n^{\mu} \nabla_{\mu} T \mathrm{d}s. \tag{91}$$

The phase arises because electronic states traverse regions of differing curvature and admissibility, unifying ESR phase shifts, spin-momentum locking, and Berry curvature in topological materials [39] [40]. Berry accumulation occurs between ESR and NMR timescales, matching the regime where CFT predicts dynamic sampling of the manifold.

Proceeding analogously to NMR, fluctuating effective fields for electronic spins arise from $\theta(t)$,

$$\delta B_{\alpha}^{(e)}(t) = b_{\alpha} \theta(t), \tag{92}$$

giving spectral densities

$$S_{\alpha\alpha}^{(e)}(\omega) = b_{\alpha}^2 \frac{2\Gamma_e k_B \Theta}{K_e^2 + (\omega\Gamma_e)^2}. \tag{93}$$

Relaxation rates then satisfy

$$\frac{1}{T_{1e}} \propto \frac{\Gamma_e}{K_e^2 + (\omega_0 \Gamma_e)^2}, \tag{94}$$

$$\frac{1}{T_{2e}} \approx \frac{1}{2T_{1e}} + \Delta\omega_{\text{aniso}}, \tag{95}$$

where $\Delta\omega_{\text{aniso}}$ is controlled by curvature-induced g-tensor and spin-orbit anisotropy. This reproduces the empirical dominance of anisotropic dephasing in heavy-element ESR [33] [35].

Within CFT, ESR and NMR are complementary probes of a single admissible ordering manifold sampled at different stiffness and coupling scales. The distinction is kinematic rather than ontological: each measures how displaced degrees of freedom relock to the same chronoscalar geometry under different admissibility costs. Orbitals provide the static baseline; ESR probes electronic phase relocking; NMR probes nuclear relocking mediated through the same manifold. The hierarchy of timescales reflects different projections of one ordering structure onto degrees of freedom with different inertia and entropy-production cost.

This unification yields predictive cross-links. Materials showing strong ESR anisotropy or holonomy must also exhibit corresponding NMR signatures—suppressed T_2, enhanced orientation dependence, and decoupling of T_1 and T_2—even when conventional mechanisms would not predict such behavior. Conversely, unusually long nuclear coherence implies stiff electronic corridors, constraining ESR response. ESR and NMR therefore form a diagnostic pair for reconstructing the same chronoscalar admissible manifold across electronic and nuclear scales.

The ESR linewidth provides the clearest electronic diagnostic of transverse admissibility microstructure. In CFT the linewidth reflects curvature variance of the

electronic ordering manifold rather than an ad hoc spin-spin parameter. Begin with the stage-1 kinematics: for an electron spin in B_0,

$$\omega_0 = g\mu_B B_0/\hbar,\ \Delta\omega_e = \sqrt{\left\langle (\delta\omega)^2 \right\rangle}.$$

In CFT the frequency shift arises from transverse curvature variation,

$$\delta\omega(x) = \Lambda_e \delta\mathcal{I}_e\left(H^{\perp}(x)\right),$$

giving

$$\Delta\omega_e = \Lambda_e \sqrt{\mathrm{Var}\left[\mathcal{I}_e\left(H^{\perp}\right)\right]}.$$

If N_{conc} shells contribute concurrently,

$$H_{ij}^{\perp} = \sum_{a=1}^{N_{\mathrm{conc}}} h_{ij}^{(a)}.$$

Yawed contributions produce anisotropy growth like a random walk,

$$\delta\lambda_{\mathrm{aniso}} \propto \sqrt{N_{\mathrm{conc}}}\, h_0,\ \mathcal{A} \propto N_{\mathrm{conc}} h_0^2,$$

so

$$\Delta\omega_e \propto N_{\mathrm{conc}}^{1/2}.$$

In heavy systems, rank reduction steepens this scaling. Introducing an amplification factor

$$\sqrt{\mathrm{Var}[\mathcal{I}_e]} \propto N_{\mathrm{conc}}^{1/2} R\left(N_{\mathrm{conc}}\right),\ R \propto N_{\mathrm{conc}}^{\alpha},$$

yields

$$\Delta\omega_e \propto N_{\mathrm{conc}}^{p},\ p = \frac{1}{2} + \alpha.$$

Values $p > 1/2$ indicate cusp-dominated transverse structure; $p \approx 1.25$ corresponds to strong rank-reduction amplification. Measuring the log-log slope

$$\frac{\mathrm{d}\ln\Delta\omega_e}{\mathrm{d}\ln N_{\mathrm{conc}}} = p$$

therefore directly probes how concurrency reshapes the transverse ordering manifold [36] [38].

This closes the predictive loop with NMR: nuclear T_1 scaling diagnoses stiffness, while ESR linewidth scaling diagnoses anisotropy and rank reduction. Together they triangulate the same chronoscalar manifold across electronic and nuclear scales using laboratory spectroscopy alone [36] [38].

13. ESR as Electronic Relocking: Spin-Orbit Curvature, Phase Stiffness, and Chronoscalar Manifold Diagnostics

Electron spin resonance (ESR) provides the electronic analogue of the nuclear relocking phenomena discussed in the preceding section. Whereas nuclear magnetic resonance probes how nuclear degrees of freedom return to admissible ordering corridors through lattice- and electron-mediated curvature, ESR probes the re-

locking of electronic spin and phase degrees of freedom themselves to the same underlying chronoscalar ordering manifold. This distinction is essential: ESR does not merely sense static orbital geometry, but directly interrogates anisotropic curvature, holonomy, and phase stiffness of the ordering field through electronic transport and coherence.

In conventional theory, ESR is described through Zeeman splitting, anisotropic g -tensors, and relaxation times derived from spin-orbit coupling, phonons, impurities, and scattering processes. This framework is experimentally validated and historically mature [33]-[36]. Chronoscalar Field Theory (CFT) does not discard this foundation; instead, it identifies the geometric object controlling those rates and anisotropies as the same admissible ordering manifold already inferred from orbital structure and nuclear relaxation.

In ESR experiments, electronic spins placed in a static magnetic field $\boldsymbol{B}_0$ absorb electromagnetic radiation at frequencies satisfying

$$\hbar\omega_0 = g\left(\hat{n}\right)\mu_B B_0, \tag{96}$$

where the g -factor depends explicitly on orientation $\hat{n}$ relative to the crystalline environment. Measured observables include resonance frequency shifts, linewidths, and longitudinal and transverse electronic relaxation times T_{1e} and T_{2e}. In heavy atoms and low-symmetry solids, these quantities are strongly anisotropic and material-specific, even when disorder is minimal [33] [34]. In particular, heavy-element systems such as tungsten, platinum, and gold exhibit broad, orientation-dependent ESR linewidths and rapid transverse decoherence, while longitudinal energy relaxation remains comparatively slow [35]-[37]. These empirical facts mirror, at the electronic level, the separation of stiffness-controlled and curvature-controlled clocks already identified in NMR.

Within CFT, electronic states are not instantaneous eigenstates but finite-support ordering configurations embedded in the chronoscalar field $T\left(x^{\mu}\right)$. The relevant coarse variable for ESR is an electronic relocking coordinate $\theta(t)$, representing the misalignment of the local electronic spin-orbital texture from an admissible ordering corridor. Perturbations such as microwave driving, band curvature, or scattering displace θ from its admissible minimum, and relaxation proceeds through dissipative relocking governed by

$$\Gamma_e\dot{\theta}(t) + K_e\theta(t) = \eta(t), \tag{97}$$

where K_e is the electronic ordering stiffness and Γ_e the electronic dissipation coefficient. The stochastic forcing $\eta(t)$ satisfies

$$\langle\eta(t)\eta(0)\rangle = 2\Gamma_e k_B\Theta\delta(t), \tag{98}$$

ensuring admissible relaxation with positive entropy production. This structure mirrors the nuclear relocking dynamics but with stiffness now controlled primarily by spin-orbit-induced curvature rather than dipolar geometry [34] [38].

In relativistic quantum mechanics, spin-orbit coupling appears as an operator proportional to $\boldsymbol{L}\cdot\boldsymbol{S}$. In CFT, the same physics is reinterpreted geometrically as

locking between electronic transport modes and anisotropic curvature of the chronoscalar manifold. Regions of strong Hessian anisotropy enforce preferred spin orientations and generate orientation-dependent g -tensor components. This interpretation accounts naturally for ESR observations in heavy atoms, where large g -factor anisotropies and linewidth broadening correlate with crystal orientation rather than impurity concentration alone [35] [39].

Electronic phase coherence further probes the geometry of the ordering manifold through holonomy. Berry phase accumulation, traditionally understood as a geometric phase in parameter or momentum space, is identified in CFT with the holonomy of chronoscalar ordering sampled by electronic phase transport,

$$\gamma_{\mathrm{B}} = \oint \mathcal{A}_i \mathrm{d}k_i \leftrightarrow \oint n^{\mu} \nabla_{\mu} T \mathrm{d}s, \tag{99}$$

where n^{μ} is the local ordering direction. This identification unifies ESR phase shifts, spin-momentum locking, and Berry curvature effects observed in heavy-element surfaces and topological materials [40]-[42]. Importantly, Berry-phase accumulation occurs on timescales intermediate between electronic hopping and nuclear relocking, precisely where CFT predicts sensitivity to curvature holonomy without full dynamical freezing.

As in the nuclear case, electronic spins couple to effective fluctuating fields generated by relocking dynamics according to

$$\delta B_{\alpha}^{(e)}(t) = b_{\alpha}\, \theta(t). \tag{100}$$

Solving the relocking equation in Fourier space yields the spectral density

$$S_{\theta\theta}(\omega) = \frac{2\Gamma_e k_B \Theta}{K_e^2 + (\omega\Gamma_e)^2}. \tag{101}$$

The electronic relaxation rates then follow

$$\frac{1}{T_{1e}} \propto \frac{\Gamma_e}{K_e^2 + (\omega_0 \Gamma_e)^2}, \tag{102}$$

$$\frac{1}{T_{2e}} \approx \frac{1}{2T_{1e}} + \Delta\omega_{\mathrm{aniso}}, \tag{103}$$

where $\Delta\omega_{\mathrm{aniso}}$ arises from spatial variation of curvature invariants across the sampled manifold. These relations predict that in stiff-manifold regimes, where $K_e \gg \omega_0 \Gamma_e$, energy relaxation is suppressed while phase coherence is dominated by curvature microstructure.

This prediction is borne out quantitatively in heavy-element systems. ESR measurements in tungsten-based materials report g -factor anisotropies of order $\Delta g \sim 0.2$ and linewidths ranging from tens to hundreds of megahertz depending on orientation [35] [39]. At a representative X-band frequency $\omega_0 \approx 2\pi \times 9.5$ GHz, a linewidth $\Delta f \sim 50$ MHz corresponds to an anisotropic dephasing scale

$$\Delta\omega_{\mathrm{aniso}} \sim 3.1 \times 10^8\ \mathrm{s}^{-1}, \tag{104}$$

far exceeding typical phonon scattering rates. This identifies anisotropic curvature, rather than stochastic disorder, as the dominant transverse dephasing mechanism.

Similar conclusions follow from studies of gold surfaces, where spin-resolved photoemission and ESR-adjacent probes reveal Rashba-type spin splitting and Berry-phase accumulation tied directly to surface orientation and band curvature [36] [41]. The effective internal fields inferred from these measurements reach several tesla, again consistent with strong yaw and rank reduction of the ordering manifold near surfaces.

CFT therefore predicts a characteristic inflection with increasing atomic number and shell concurrency. As concurrency increases, electronic stiffness K_e grows due to baryonic stiffening and overlapping shell curvature, while curvature anisotropy simultaneously increases. The result is a regime in which T_{1e} grows with stiffness while T_{2e} collapses due to curvature variance,

$$T_{1e} \propto K_e^2, \; T_{2e}^{-1} \propto \sqrt{\mathrm{Var}\left[\mathcal{I}\left(H\right)\right]}. \tag{105}$$

This simultaneous stiffening and fragilization is not paradoxical but diagnostic of a rank-reduced, anisotropic ordering manifold.

The strongest tests of this framework arise in systems where ESR and NMR can be measured within the same material. In transition-metal-doped semiconductors and heavy-element crystals, ESR probes electronic curvature and holonomy directly, while NMR probes nuclear relocking mediated by the same curvature. CFT predicts that stiffness parameters inferred from T_{1e} and T_1 should scale consistently, while anisotropy parameters inferred from ESR linewidths and NMR dephasing should correlate through the same curvature invariants.

Orbitals diagnose the static admissible manifold, ESR diagnoses electronic phase relocking and holonomy, and NMR diagnoses nuclear relocking through the same curvature. These are not separate phenomena, but complementary probes of a single ordering structure sampled at different dynamical scales. The unification of these probes is the central predictive strength of the chronoscalar framework.

14. Josephson Dynamics as Macroscopic Phase Relocking: Superconducting Stiffness, Chronoscalar Torsion, and Collective Ordering

Josephson phenomena provide the macroscopic limit of the relocking dynamics developed in the previous atomic and electronic sections. Whereas NMR probes nuclear relocking mediated by electronic curvature, and ESR probes electronic relocking governed by spin-orbit anisotropy and holonomy, Josephson junctions probe the collective relocking of a macroscopic phase field. This phase is conventionally interpreted as the superconducting order parameter, but in Chronoscalar Field Theory (CFT) it is identified as a large-scale, coherent relocking coordinate constrained by the same admissible ordering manifold that governs atomic orbitals, electronic spin coherence, and nuclear relaxation.

In standard superconductivity theory, Josephson effects arise from the phase difference $\Delta\varphi$ between two superconductors separated by a weak link. The defining relations,

$$I = I_c \sin \Delta\varphi, \quad \hbar \frac{\mathrm{d}\Delta\varphi}{\mathrm{d}t} = 2eV, \tag{106}$$

are experimentally exact and have been confirmed across a wide range of materials and junction geometries [43]-[45]. These relations are typically derived from microscopic pairing theory or phenomenological Ginzburg-Landau arguments. CFT does not dispute these results; instead, it identifies the geometric origin of the phase variable itself and the physical meaning of the stiffness and dissipation parameters that control its dynamics.

In the chronoscalar framework, the superconducting phase $\varphi(x,t)$ is not an abstract quantum angle but a coarse-grained ordering coordinate describing how a macroscopic condensate is aligned with an admissible chronoscalar corridor. A Josephson junction forces two such ordered regions to share a boundary across which admissibility must be restored dynamically. The phase difference $\Delta\varphi(t)$ is therefore a measurable manifestation of relocking between two large, stiff ordering domains.

The minimal admissible dynamics of $\Delta\varphi$ follow directly from the same finite-support and entropy-production principles applied earlier. For a current-biased junction, the relocking equation takes the form

$$C \frac{\mathrm{d}^2\Delta\varphi}{\mathrm{d}t^2} + \frac{1}{R}\frac{\mathrm{d}\Delta\varphi}{\mathrm{d}t} + K_J \sin \Delta\varphi = I_{\mathrm{ext}}, \tag{107}$$

where C is the junction capacitance, R the shunt resistance, and K_J the Josephson stiffness proportional to the critical current I_c. Equation (107) is usually introduced as the resistively and capacitively shunted junction (RCSJ) model [44]. In CFT, it is reinterpreted as the overdamped or underdamped relocking equation for a macroscopic ordering coordinate constrained by admissibility.

The key identification is that K_J plays the same structural role as the stiffness parameters K and K_e introduced for nuclear and electronic relocking. It quantifies the energetic cost of misalignment between two admissible ordering manifolds. Importantly, K_J is not an arbitrary parameter; it scales with the density of Cooper pairs and therefore with the stiffness of the underlying chronoscalar field in the superconducting state.

Small deviations from equilibrium, $\Delta\varphi \ll 1$, linearize (107) to

$$C\ddot{\Delta}\varphi + \frac{1}{R}\dot{\Delta}\varphi + K_J \Delta\varphi = I_{\mathrm{ext}}. \tag{108}$$

In the overdamped regime relevant to most DC Josephson experiments, inertial effects are negligible and the relocking time is

$$\tau_J \sim \frac{R}{K_J}. \tag{109}$$

This expression makes explicit that the Josephson relaxation time is set by a ratio of dissipation to stiffness, exactly as in the nuclear and electronic cases.

The chronoscalar interpretation becomes particularly sharp when one considers phase noise and linewidth in Josephson oscillations. Experimentally, the AC Josephson effect produces radiation at frequency

$$f_J = \frac{2e}{h}V, \tag{110}$$

with a finite linewidth determined by thermal noise, junction geometry, and material properties [45] [46]. In CFT, this linewidth is identified with fluctuations of the relocking coordinate driven by admissible noise, leading to a phase-diffusion spectrum

$$S_{\varphi\varphi}(\omega) = \frac{2\Gamma_J k_B \Theta}{K_J^2 + (\omega\Gamma_J)^2}, \tag{111}$$

where $\Gamma_J \sim 1/R$ is the macroscopic dissipation coefficient. The resulting linewidth scales inversely with K_J, predicting that stiffer superconductors exhibit narrower Josephson emission lines, a trend well established experimentally [46] [47].

The predictive content of CFT becomes especially clear when comparing different superconducting materials. Conventional low-T_c superconductors such as aluminum exhibit relatively small K_J, modest critical currents, and strong sensitivity to thermal noise. In contrast, transition-metal superconductors and cuprate materials exhibit much larger critical currents and correspondingly higher stiffness. Experiments on niobium and YBCO junctions report linewidth reductions of more than an order of magnitude compared to aluminum-based devices at comparable temperatures, consistent with a quadratic or stronger dependence of coherence on stiffness [47] [48].

CFT predicts that this scaling is not merely a materials detail but reflects increasing baryonic stiffening and shell concurrency at the electronic level. The same shell concurrency that increases electronic stiffness K_e in ESR also increases macroscopic stiffness K_J in the superconducting state. This leads to a consistent hierarchy:

$$K_{\text{orbital}} \ll K_e \ll K_J, \tag{112}$$

with corresponding increases in coherence length and decreases in admissible phase noise.

Josephson vortices and flux quantization provide a further geometric diagnostic. In standard theory, flux quantization follows from single-valuedness of the superconducting wavefunction. In CFT, it follows from the admissibility of closed relocking loops in the chronoscalar manifold. The quantization condition

$$\oint \nabla\varphi \cdot \mathrm{d}\ell = 2\pi n \tag{113}$$

is reinterpreted as a holonomy constraint on the ordering field, directly analogous to Berry-phase accumulation in ESR and to nodal structure in atomic orbitals [49]. The appearance of quantized fluxoids is therefore not a purely quantum postulate but a geometric necessity of admissible relocking.

Experimental observations of anisotropic Josephson critical currents in layered superconductors further support this view. Measurements on cuprates show that I_c varies strongly with junction orientation relative to crystal axes, indicating an-

isotropic phase stiffness tied to underlying electronic structure [48] [50]. CFT predicts exactly this behavior, since anisotropic curvature of the ordering manifold reduces admissible transport in certain directions, lowering effective stiffness.

The strongest triangulation of the chronoscalar framework arises in systems where all three probes are available. In heavy-element superconductors such as Nb or Pb, atomic orbitals show strong shell concurrency, ESR reveals large g-tensor anisotropy and rapid transverse decoherence, NMR exhibits long T_1 with curvature-dominated dephasing, and Josephson junctions display high critical currents and narrow linewidths. These observations are typically treated as unrelated material properties. In CFT they are unified as successive manifestations of the same ordering manifold sampled at increasing spatial and temporal scales.

Orbitals diagnose static internal imaging geometry, ESR diagnoses electronic phase relocking and holonomy, NMR diagnoses nuclear relocking mediated by electronic curvature, and Josephson dynamics diagnose macroscopic collective relocking. The Josephson effect therefore closes the experimental hierarchy, demonstrating that chronoscalar ordering persists coherently from atomic to macroscopic scales without invoking new postulates or scale-dependent laws.

15. Meissner Effect as Torsion Exclusion: Chronoscalar Stiffness, Boundary Admissibility, and Flux Expulsion

The Meissner effect marks the final stage in the chronoscalar ordering hierarchy. Earlier sections described how admissible manifolds respond to disturbance through *relocking*: orbitals stabilize internal imaging modes, ESR and NMR measure local return to admissibility, and Josephson dynamics describe macroscopic phase relocking. In the superconducting state, however, relocking is no longer the dominant response. Instead, inadmissible transverse curvature is expelled from the ordered region altogether. The Meissner effect is therefore not merely a property of superconductivity; it is the macroscopic manifestation of *torsion exclusion* enforced by chronoscalar admissibility.

Experimentally, a superconductor below its critical temperature expels magnetic flux from its interior, independent of magnetic history. This distinguishes superconductors from perfect conductors and was first demonstrated by Meissner and Ochsenfeld [51]. Conventional theory encodes the phenomenon in the London equations [52], which yield

$$\nabla^2 \boldsymbol{B} = \frac{1}{\lambda_L^2} \boldsymbol{B}, \tag{114}$$

so magnetic fields decay exponentially inside a superconductor with penetration depth

$$\lambda_L = \sqrt{\frac{m}{\mu_0 n_s e^2}}. \tag{115}$$

These relations describe observations but do not explain why equilibrium bulk flux is inadmissible rather than merely persistent.

In Chronoscalar Field Theory (CFT), magnetic flux corresponds to torsional curvature of admissible ordering corridors. In the normal state the ordering manifold is sufficiently soft to accommodate such curvature. In the superconducting state, collective phase coherence dramatically increases the ordering stiffness K, and admissibility forbids sustained internal torsion. The system therefore restores admissibility by expelling torsion from the bulk and confining it to a boundary layer.

This follows directly from the chronoscalar action. Electromagnetic transport couples to the ordering gradient through

$$\mathcal{L}_{\text{int}} \sim \left(1+\kappa\rho_b\right)\left|\nabla T-\alpha \boldsymbol{A}\right|^2, \tag{116}$$

where α fixes the coupling scale. Minimizing the free energy in the stiff-manifold regime yields

$$\nabla\times\nabla\times\boldsymbol{A}=\frac{1}{\lambda^2}\boldsymbol{A},\ \ \lambda^{-2}\propto K, \tag{117}$$

identifying the penetration depth as the geometric thickness over which the manifold transitions from torsion-free interior to admissible exterior transport. The London result is thus recovered, but interpreted as a stiffness-driven admissibility constraint rather than a phenomenological postulate.

This interpretation immediately explains the history independence of flux expulsion. Once the manifold closes into a globally admissible state, any configuration containing bulk torsion is forbidden regardless of its origin. The Meissner effect is therefore not a dissipative relaxation process like NMR or Josephson relocking, but a geometric exclusion enforced by manifold admissibility [53].

Flux quantization follows from the same logic. In multiply connected geometries, complete torsion exclusion is impossible; admissibility permits only discrete holonomy states,

$$\oint n^{\mu}\nabla_{\mu}T\mathrm{d}s=2\pi N, \tag{118}$$

reproducing quantized fluxoids [54]-[56] as the minimal torsion-compatible circulation of the ordering field.

Anisotropic and unconventional superconductors fit naturally into this framework. Direction-dependent stiffness K_i produces tensorial penetration depths,

$$\lambda_i^{-2}\propto K_i, \tag{119}$$

as observed in cuprates and heavy-fermion materials [57] [58]. Torsion exclusion thus becomes axis-dependent, yielding partial flux penetration and orientation-sensitive screening.

The predictive strength of this picture lies in its unification of stiffness diagnostics. The same stiffness parameter governing Josephson plasma frequency, NMR T_1 scaling, and ESR linewidth collapse also sets penetration depth and flux exclusion strength. Materials with large K exhibit short λ_L, strong Meissner screening, long T_1, and high phase rigidity, while anisotropic or reduced K produces weakened screening and enhanced transverse microstructure effects [59].

The Meissner effect therefore completes the relocking hierarchy. Orbitals admit internal imaging, ESR and NMR admit local relocking, Josephson dynamics admit macroscopic phase relocking, and the superconducting state admits no internal torsion at all. What appears electromagnetically as flux expulsion is, at the ordering level, the inevitable geometric consequence of a chronoscalar manifold whose stiffness has exceeded the threshold for sustaining transverse curvature.

16. Aharonov-Bohm Effect as Global Admissibility Constraint

The Aharonov-Bohm (AB) effect provides the clearest experimental demonstration that transport can be governed by global ordering constraints even when all local forces vanish. In its canonical form, a charged particle propagates through a region of space in which the magnetic field $\boldsymbol{B}$ is identically zero, yet the interference phase depends on magnetic flux confined to an excluded region. The original theoretical formulation and subsequent experiments established that the phase of a transported state is sensitive to global topology rather than local curvature alone [60]-[62].

Within Chronoscalar Field Theory (CFT), the AB effect is neither paradoxical nor evidence for the primacy of gauge potential. Instead, it is the archetypal example of a *global admissibility constraint*: transport is locally admissible everywhere along the path, but global closure of the ordering manifold enforces a non-removable phase condition. Unlike the Meissner effect, which suppresses curvature locally through stiffness, the AB effect operates in the opposite limit—where local curvature vanishes identically and only global ordering remains.

In standard quantum mechanics, the AB phase acquired by a particle of charge q traversing a closed path $\mathcal{C}$ is

$$\Delta\varphi_{\mathrm{AB}} = \frac{q}{\hbar}\oint_{\mathcal{C}} \boldsymbol{A}\cdot \mathrm{d}\ell = \frac{q}{\hbar}\Phi, \tag{120}$$

where Φ is the magnetic flux enclosed by $\mathcal{C}$. The magnetic field vanishes along the path, $\boldsymbol{B} = \nabla\times\boldsymbol{A} = 0$, yet the phase is finite and experimentally measurable [61] [63]. This expression is exact, but it does not identify what physical structure enforces the phase constraint once local fields are removed.

CFT identifies the relevant structure as the global admissibility class of the chronoscalar ordering manifold. Transport occurs along corridors defined by the scalar ordering field $T\left(x^{\mu}\right)$, and phase accumulation reflects the integral of an effective ordering connection $\mathcal{A}_{\mu}$ along the transport path. Crucially, this connection is not required to have local curvature; admissibility requires only that the ordering corridor close consistently in the presence of global exclusion.

The accumulated ordering phase along a trajectory $\mathcal{C}$ is therefore written as

$$\Theta[\mathcal{C}] = \int_{\mathcal{C}} \mathcal{A}_{\mu}\mathrm{d}x^{\mu}, \tag{121}$$

with $\nabla\times\mathcal{A} = 0$ everywhere accessible to the particle. If the ordering manifold is simply connected, $\Theta[\mathcal{C}]$ can be continuously deformed to zero. If the manifold

is multiply connected, $\Theta[\mathcal{C}]$ is topologically protected and cannot be removed by any local deformation.

The AB phase is therefore a holonomy of the ordering manifold. This immediately explains why shielding the magnetic field does not eliminate the effect: shielding removes local curvature but does not alter the global admissibility class. As long as the excluded region remains topologically nontrivial, the ordering corridor winds nontrivially and the accumulated phase remains fixed. This is precisely what is observed experimentally, even when the magnetic field is confined within superconducting shields [62].

The predictive content of CFT becomes explicit when one considers coherence length and energy scaling. The AB phase is observable only if transport remains coherent around the loop. Let L denote the loop circumference and ℓ_ϕ the phase coherence length. The visibility $\mathcal{V}$ of the interference pattern scales as

$$\mathcal{V}(L) \sim \exp\left(-\frac{L}{\ell_\phi}\right), \tag{122}$$

while the phase shift itself remains exactly $\Delta\varphi_{\mathrm{AB}}$ so long as coherence is maintained. CFT predicts that ℓ_ϕ is controlled by the same admissibility-relaxation mechanisms identified in NMR and ESR, but the phase magnitude is not renormalized by decoherence—only its observability is suppressed.

This distinction is borne out in mesoscopic ring experiments in normal metals and semiconductors, where AB oscillations persist up to temperatures and disorder levels far above those required for superconductivity [61] [64]. In these systems, local stiffness is negligible, yet global ordering remains coherent over mesoscopic scales. CFT therefore predicts that AB-type oscillations should be observable in any system where the chronoscalar ordering corridor remains globally coherent over a closed loop, independent of whether a condensate or gap exists.

A particularly clean quantitative example is provided by metallic rings of radius $R \sim 1\,\mu\mathrm{m}$. The fundamental AB oscillation period corresponds to one flux quantum $\Phi_0 = h/q$, producing conductance oscillations with period

$$\Delta B = \frac{\Phi_0}{\pi R^2}. \tag{123}$$

This relation is purely geometric and contains no material parameters beyond the carrier charge. CFT interprets this universality as direct evidence that the phase constraint is imposed by global admissibility rather than by local interaction strength. Changes in material composition affect ℓ_ϕ and therefore visibility, but not the oscillation period itself.

The AB effect also provides a direct bridge to Berry phase phenomena. When the ordering manifold varies smoothly rather than being strictly excluded, the holonomy becomes geometric rather than topological. In that limit, the accumulated phase depends on the integral of curvature over parameter space rather than on a winding number. CFT treats both cases within the same framework: the AB effect corresponds to a discrete admissibility class, while Berry phases correspond to

continuous admissibility curvature. The distinction is quantitative, not conceptual [65]-[68].

A falsifiable prediction follows immediately. Consider a mesoscopic ring fabricated from a material with strong anisotropic ordering microstructure. CFT predicts that while the AB oscillation period remains fixed by geometry, the phase coherence length ℓ_ϕ will exhibit orientation dependence relative to the underlying ordering manifold, analogous to the orientation-dependent linewidths observed in NMR. This anisotropy should appear as direction-dependent suppression of AB visibility without any change in oscillation period. Such effects have already been reported in quasi-one-dimensional conductors and layered materials, though they are not typically interpreted in this unified framework [66] [68].

In summary, the Aharonov-Bohm effect is the limiting case of transport governed purely by global admissibility. Where orbitals diagnose static imaging structure, NMR diagnoses local relocking, and the Meissner effect enforces torsion exclusion through stiffness, the AB effect demonstrates that even in the complete absence of local curvature, global ordering closure constrains phase and transport. No additional machinery is required beyond the chronoscalar ordering manifold already introduced; the AB effect is simply its global, curvature-free manifestation.

17. Topological Insulators as Boundary-Locked Admissibility Corridors

Topological insulators provide the natural continuation of the Aharonov-Bohm paradigm: whereas the AB effect demonstrates phase constraint through global exclusion with no local curvature, topological insulators demonstrate *persistent transport constrained to boundaries* despite the presence of a gapped bulk. In standard condensed-matter language, this phenomenon is attributed to topological band invariants and spin-orbit coupling. In Chronoscalar Field Theory (CFT), the same observations are reinterpreted as a manifestation of boundary-locked admissibility corridors: transport is forbidden in the bulk ordering manifold but remains admissible along lower-dimensional boundary closures enforced by global ordering consistency.

Experimentally, three-dimensional topological insulators exhibit an insulating bulk with conducting two-dimensional surface states, while two-dimensional topological insulators exhibit one-dimensional edge channels. These channels are robust against disorder, weak interactions, and smooth deformations, provided that global symmetries are preserved [69]-[72]. The persistence of boundary transport in the absence of bulk conduction is the central phenomenon to be explained.

In conventional theory, the bulk Hamiltonian admits a topological invariant—such as a Chern number or $\mathbb{Z}_2$ index—that guarantees the existence of gapless boundary modes. While mathematically correct, this description leaves open the physical question of *why* transport is allowed on the boundary but not in the bulk. CFT answers this by identifying the bulk as an inadmissible ordering region and the boundary as a lower-rank admissible closure of the chronoscalar ordering manifold.

Let the chronoscalar field $T\left(x^{\mu}\right)$ define an ordering manifold whose admissibility requires finite-support transport corridors. In a topological insulator, strong spin-orbit coupling and lattice-induced anisotropy generate a bulk ordering curvature that renders extended transport inadmissible. This is expressed geometrically as a positive mass gap Δ in the bulk spectrum, corresponding to a stiffness barrier in the ordering manifold. However, at the boundary, the ordering manifold undergoes rank reduction: one spatial degree of freedom collapses, allowing admissible transport along the remaining tangential directions.

This structure is encoded mathematically by an effective Dirac-type Hamiltonian for surface states,

$$H_{\text{surf}} = v_F \left(\boldsymbol{\sigma} \times \boldsymbol{k}\right) \cdot \hat{\boldsymbol{n}}, \tag{124}$$

where $\hat{\boldsymbol{n}}$ is the surface normal. In CFT, this Hamiltonian is not fundamental; it is the effective description of a boundary admissibility corridor whose orientation is fixed by the ordering manifold's closure. The absence of backscattering follows because reversal would require transport through the bulk inadmissible region, which is geometrically forbidden.

The robustness of boundary transport can be quantified by examining the penetration depth of surface states into the bulk. Experimentally, this decay length λ is given by

$$\lambda \sim \frac{\hbar v_F}{\Delta}, \tag{125}$$

where Δ is the bulk gap [70] [73]. CFT interprets λ as the characteristic scale over which admissibility transitions from allowed (boundary) to forbidden (bulk). Importantly, this scale is geometric and ordering-based, not dynamical: increasing disorder or reducing mobility does not eliminate the surface state unless the admissibility class itself is altered.

A canonical physical example is Bi_2Se_3, whose surface states have been directly imaged by angle-resolved photoemission spectroscopy (ARPES). These experiments reveal linear Dirac dispersion with a single Dirac cone per surface and penetration depths on the order of a few nanometers [69] [71]. From a CFT perspective, this indicates a sharply defined admissibility boundary where curvature changes sign and rank is reduced. The existence of a single Dirac cone reflects the minimal admissible closure consistent with global ordering.

The predictive power of the CFT reinterpretation becomes evident when considering perturbations. In standard theory, breaking time-reversal symmetry opens a gap in the surface spectrum. In CFT, this corresponds to lifting the boundary admissibility by reintroducing curvature that closes the corridor. Magnetic doping of Bi_2Se_3 provides a direct experimental test: surface states acquire a mass gap while the bulk remains insulating [72]. This is precisely the behavior expected when the boundary ordering manifold is rendered inadmissible by additional curvature.

CFT further predicts that not all boundaries are equivalent. The admissibility of a boundary corridor depends on its orientation relative to the underlying or-

dering manifold. This leads to anisotropic surface transport, even in materials with nominally isotropic bulk band structures. Such anisotropies have been observed experimentally as direction-dependent surface velocities and scattering rates in both three-dimensional and two-dimensional topological insulators [74] [75].

A quantitative prediction follows by relating boundary stiffness to surface-state velocity. Let $K_{\parallel}$ denote the effective stiffness along the boundary corridor. Then the surface-state velocity satisfies

$$v_F \propto \sqrt{K_{\parallel}}, \tag{126}$$

analogous to the stiffness-controlled scaling derived for NMR relaxation. Variations in lattice termination, strain, or chemical composition that modify $K_{\parallel}$ should therefore produce measurable shifts in v_F without closing the bulk gap. This prediction is consistent with observed velocity renormalization under strain and substrate interaction.

The connection to the Aharonov-Bohm effect is now transparent. In AB systems, global admissibility constrains phase accumulation in the absence of local curvature. In topological insulators, global admissibility constrains *where transport may occur*. The boundary is not merely a geometric edge; it is the locus where admissibility survives dimensional reduction. Transport persists not because the boundary is special, but because it is the only region where ordering closure remains possible.

In summary, topological insulators realize boundary-locked admissibility corridors. Bulk transport is suppressed by ordering curvature, while boundary transport survives as a lower-dimensional closure of the chronoscalar manifold. The observed robustness, anisotropy, and response to symmetry-breaking perturbations follow directly from admissibility logic and require no additional postulates beyond those already established for orbitals, NMR, the Meissner effect, and the Aharonov-Bohm phenomenon.

18. Berry Phase as Ordering Holonomy

The Berry phase represents the continuous, curvature-resolved limit of the global admissibility constraints previously illustrated by the Aharonov-Bohm effect and boundary-locked transport in topological insulators. Whereas the Aharonov-Bohm phase arises from transport around an excluded region with vanishing local curvature, and topological insulators arise from admissible closure at a boundary where bulk transport is forbidden, the Berry phase arises when transport occurs through a *smoothly varying admissible manifold*. In this regime, phase accumulation reflects not topology alone, but the distributed geometry of the ordering field.

In standard quantum mechanics, the Berry phase is defined for a system whose Hamiltonian $H(\boldsymbol{\lambda})$ depends adiabatically on a set of parameters $\boldsymbol{\lambda}$. When the parameters trace a closed loop $\mathcal{C}$ in parameter space, an eigenstate $|n(\boldsymbol{\lambda})\rangle$ ac-

quires a geometric phase

$$\gamma_n[\mathcal{C}] = i\oint_{\mathcal{C}} \langle n(\boldsymbol{\lambda}) | \nabla_{\boldsymbol{\lambda}} n(\boldsymbol{\lambda}) \rangle \cdot \mathrm{d}\boldsymbol{\lambda}, \tag{127}$$

in addition to the usual dynamical phase. This phase depends only on the geometry of the path in parameter space, not on the rate at which it is traversed, provided adiabaticity holds [76].

Within Chronoscalar Field Theory (CFT), the Berry phase is reinterpreted as an explicit *ordering holonomy*. The relevant parameter space is not abstract; it is the space of admissible orientations and curvatures of the chronoscalar ordering manifold. As a system is transported through a family of admissible configurations, the ordering corridor twists continuously. The accumulated phase is the integral of this twist, precisely analogous to parallel transport on a curved manifold.

To make this explicit, let $\mathcal{M}$ denote the space of admissible ordering configurations parameterized by coordinates λ^a. The chronoscalar ordering connection $\mathcal{A}_a$ is defined as the generator of infinitesimal relocking under variation of λ^a. The accumulated phase is then

$$\Theta[\mathcal{C}] = \oint_{\mathcal{C}} \mathcal{A}_a(\boldsymbol{\lambda}) \mathrm{d}\lambda^a, \tag{128}$$

which is formally identical to (127), but with a concrete physical interpretation: $\mathcal{A}_a$ encodes the local orientation of the admissible ordering manifold rather than an abstract gauge freedom.

The associated curvature,

$$\mathcal{F}_{ab} = \partial_a \mathcal{A}_b - \partial_b \mathcal{A}_a, \tag{129}$$

measures the failure of relocking operations to commute. In CFT this non-commutativity is not an algebraic artifact; it reflects the physical fact that ordering relocking along different directions of parameter space does not close trivially when curvature is present. The Berry curvature is therefore a direct probe of distributed admissibility curvature.

A canonical physical example is provided by spin-1/2 particles in a slowly varying magnetic field. In the conventional picture, a spin adiabatically following a magnetic field $\boldsymbol{B}$ acquires a Berry phase equal to half the solid angle subtended by the field trajectory on the Bloch sphere [76] [77]. In CFT terms, the magnetic field defines a slowly rotating ordering axis, and the spin remains locked to the admissible corridor defined by that axis. The accumulated phase measures the total yaw of the ordering manifold during the cycle.

This interpretation becomes predictive when extended to crystalline solids. In Bloch-band systems, the Berry curvature in momentum space governs anomalous velocities, Hall responses, and orbital magnetization [78]. CFT reinterprets momentum-space Berry curvature as the projection of real-space ordering curvature onto transport corridors. The anomalous Hall conductivity,

$$\sigma_{xy} = \frac{e^2}{\hbar} \int_{\mathrm{BZ}} \frac{\mathrm{d}^3 k}{(2\pi)^3} \Omega_{xy}(\boldsymbol{k}), \tag{130}$$

is therefore read not merely as a band-topological invariant, but as an integrated

measure of ordering holonomy over the admissible transport manifold.

This perspective clarifies why Berry curvature effects are robust against disorder that preserves global admissibility. Local scattering perturbs trajectories but does not alter the integrated curvature unless the admissibility class itself changes. This robustness is experimentally confirmed in anomalous Hall systems and in materials exhibiting large Berry curvature "hot spots" near avoided crossings [79] [80].

A particularly clean atomic-scale example is provided by molecular systems undergoing cyclic distortions, such as the Jahn-Teller effect. In these systems, adiabatic nuclear motion around a conical intersection produces a Berry phase of π, observable as a sign change in the electronic wavefunction [81]. In CFT language, the conical intersection represents a localized curvature singularity in the ordering manifold, and the Berry phase reflects the unavoidable holonomy induced by encircling it. This is the molecular analogue of the Aharonov-Bohm effect, with curvature distributed rather than excluded.

CFT makes a quantitative prediction that extends beyond standard treatments. Because the ordering manifold is physical, not abstract, its curvature must also influence relaxation and dephasing. Systems with large Berry curvature are therefore predicted to exhibit enhanced sensitivity in relocking dynamics, producing correlated signatures in transport coefficients and coherence times. For example, materials with sharply peaked Berry curvature should show orientation-dependent dephasing analogous to that observed in NMR, even when conventional spin-orbit scattering is weak.

This prediction can be tested by comparing Berry-curvature maps from angle-resolved photoemission or first-principles calculations with experimentally measured anisotropies in quantum oscillations or weak localization corrections. CFT predicts that maxima in Berry curvature correspond to regions of reduced relocking stiffness and enhanced phase fragility, a correspondence that is beginning to emerge in correlated and topological materials [79] [82].

In summary, the Berry phase is the smooth-curvature limit of ordering holonomy. It unifies the discrete global phase of the Aharonov-Bohm effect, the boundary-locked transport of topological insulators, and the distributed curvature of band and molecular systems into a single geometric principle: admissible ordering manifolds accumulate phase when transported through curvature. Within CFT, the Berry phase is not an abstract gauge artifact but a measurable imprint of chronoscalar ordering geometry.

Experimental Anchors and Prior Berry-Phase Realizations

The geometric phase phenomena discussed above are not introduced as novel observations but as established experimental facts whose interpretation is reorganized within Chronoscalar Field Theory. For clarity and intellectual traceability, we list here the canonical experimental realizations that anchor the discussion.

The existence of a Berry phase associated with nuclear motion around conical

intersections in molecular systems was established through spectroscopic measurements demonstrating a sign change in vibrational wavefunctions under adiabatic transport in configuration space. Early theoretical formulation and experimental confirmation appear in the work of Berry and Wilkinson, Herzberg and Longuet-Higgins, and subsequent high-resolution molecular spectroscopy studies [69]-[72]. These systems provide a real-space realization of geometric holonomy without reliance on band structure, transport currents, or magnetic ordering.

Berry phases associated with spin transport were directly measured in neutron interferometry experiments, where polarized neutron beams acquire a phase proportional to the solid angle traced on the Bloch sphere under adiabatic evolution of the magnetic field orientation [73]-[75]. These experiments constitute a clean demonstration of geometric phase accumulation in spin space and serve as a non-electronic, non-solid-state anchor for ordering holonomy.

More recently, synthetic gauge fields engineered in ultracold atomic systems have enabled direct mapping of Berry curvature and geometric phases under controlled deformation of the underlying Hamiltonian [76]-[79]. In these platforms, Berry curvature is measured through transverse drift and anomalous velocity responses, allowing direct experimental access to geometric quantities that are otherwise inferred indirectly in condensed-matter systems.

Phenomena associated with Berry curvature-driven transport in itinerant ferromagnets and Dirac materials, including anomalous Hall responses, have been treated in separate work and are not repeated here. The present section focuses exclusively on Berry phases arising from admissible ordering holonomy rather than curvature-weighted transport coefficients.

19. Mathematical Derivation of the Machian Degrees-of-Freedom Split in CFT

Chronoscalar Field Theory (CFT) treats time as a physical ordering scalar $T\left(x^{\mu}\right)$ whose nonvanishing gradient defines a preferred local ordering direction. The Machian degrees-of-freedom (DoF) split is not postulated; it is forced by: 1) a timelike ordering gradient, 2) admissibility (finite support and nonnegative ordering entropy production), and 3) global sourcing of the ordering field by matter through a nonlocal Mach functional. The result is a sharp decomposition into one longitudinal streaming DoF and three transverse shear DoF with distinct admissibility costs.

Assume the ordering gradient is timelike on the domain of interest,

$$X \equiv -\nabla_{\mu} T \nabla^{\mu} T > 0.$$

Define the normalized ordering direction

$$n_{\mu} \equiv \frac{\nabla_{\mu} T}{\sqrt{X}}, \quad n_{\mu} n^{\mu} = -1,$$

where $g_{\mu\nu}$ is used only as a bilinear form to raise/lower indices and define orthogonality; no GR field equations are invoked. The orthogonal projector

$$P_{\mu\nu} \equiv g_{\mu\nu} + n_\mu n_\nu,\ P_{\mu\nu} n^\nu = 0,\ P^\mu{}_\mu = 3,$$

establishes the DoF split kinematically: a rank-1 longitudinal subspace spanned by n^μ and a rank-3 transverse subspace orthogonal to it.

Any covector A_μ decomposes uniquely,

$$A_\mu = A_\mu^{\parallel} + A_\mu^{\perp},\ A_\mu^{\parallel} \equiv -\left(A_\nu n^\nu\right) n_\mu,\ A_\mu^{\perp} \equiv P_\mu{}^\nu A_\nu.$$

For a scalar κ,

$$\left(\nabla_\mu \kappa\right)^{\parallel} = -\left(n^\nu \nabla_\nu \kappa\right) n_\mu,\ \left(\nabla_\mu \kappa\right)^{\perp} = P_\mu{}^\nu \nabla_\nu \kappa.$$

This is the mathematical content of the 1 + 3 Machian split: one ordering direction and three transverse deformation directions.

Take a minimal CFT ordering action

$$S_T[T] = \int \mathrm{d}^4 x \sqrt{-g}\, \mathcal{L}_T(T, X),\ X \equiv -\nabla_\mu T \nabla^\mu T,$$

with a matter coupling that may be nonlocal in the Machian sense,

$$S = S_T[T] + S_{\mathrm{M}}[T; \rho].$$

Variation yields

$$\nabla_\mu\left(\mathcal{L}_X \nabla^\mu T\right) - \mathcal{L}_T = \mathcal{J}_{\mathrm{M}}[T; \rho],\ \mathcal{L}_X \equiv \frac{\partial \mathcal{L}_T}{\partial X},\ \mathcal{L}_T \equiv \frac{\partial \mathcal{L}_T}{\partial T}.$$

The Mach source $\mathcal{J}_{\mathrm{M}}$ is defined by nonlocal participation of matter,

$$\mathcal{J}_{\mathrm{M}}(x) = \int \mathrm{d}^4 x' \sqrt{-g(x')}\, \mathcal{K}(x, x') \rho(x') \Xi\left(T(x), T(x')\right),$$

so distant matter contributes to setting the local ordering corridor. Because $\nabla_\mu T$ is the only preferred first-derivative direction in the action, all admissibility costs resolve into components parallel and perpendicular to n_μ.

Define the ordering Hessian

$$H_{\mu\nu} \equiv \nabla_\mu \nabla_\nu T,$$

and decompose it as

$$H_{\mu\nu} = \left(n_\mu n_\nu\right) H_{\parallel\parallel} + 2 n_{(\mu} H_{\nu)\parallel\perp} + H_{\mu\nu}^{\perp},$$

where

$$H_{\parallel\parallel} = n^\mu n^\nu H_{\mu\nu},\ H_{\mu\parallel\perp} = -P_\mu{}^\alpha n^\beta H_{\alpha\beta},\ H_{\mu\nu}^{\perp} = P_\mu{}^\alpha P_\nu{}^\beta H_{\alpha\beta}.$$

This is the curvature-support split into streaming (longitudinal) and shear/shape (transverse) components. In CFT, irreversibility and dissipation reside in the rank-3 transverse sector, where admissibility can fail via shear, winding, and corridor microstructure.

Admissibility constrains allowable histories of T. Finite support forbids arbitrarily instantaneous evolution along the ordering direction. Nonnegative ordering entropy production requires an entropy current s_T^μ with

$$\nabla_\mu s_T^\mu = \sigma_T \geq 0.$$

Structurally, σ_T must vanish for pure longitudinal streaming and grow with

transverse deformation. A minimal admissible class is

$$\sigma_T = \gamma_1 H^{\perp}_{\mu\nu} H^{\perp\mu\nu} + \gamma_2 \left(\mathrm{tr} H^{\perp}\right)^2 + \gamma_3 \mathcal{A}\left(H^{\perp}\right),\ \gamma_i \geq 0,$$

where $\mathcal{A}\left(H^{\perp}\right)$ is an anisotropy invariant built from eigenvalue differences of $H^{\perp}$. Longitudinal motion is therefore low-entropy streaming; transverse deformation carries ordering cost.

The Machian content now becomes explicit: the global source $\mathcal{J}_{\mathrm{M}}$ selects the local corridor, fixing which variations are inexpensive (longitudinal) and which are costly (transverse). Define an ordering flux

$$J^{\mu} = \mathcal{L}_X \nabla^{\mu} T = \mathcal{L}_X \sqrt{X}\, n^{\mu}.$$

The field equation becomes

$$\nabla_{\mu} J^{\mu} - \mathcal{L}_T = \mathcal{J}_{\mathrm{M}}.$$

Projecting along n^{μ} governs streaming/relaxation of X,

$$n_{\mu} \nabla_{\nu} \left(\mathcal{L}_X \nabla^{\nu} T\right) - n_{\mu} \mathcal{L}_T = n_{\mu} \mathcal{J}_{\mathrm{M}},$$

while the transverse projection governs corridor shape and microstructure,

$$P_{\mu}{}^{\alpha} \nabla_{\nu} \left(\mathcal{L}_X \nabla^{\nu} T\right) = P_{\mu}{}^{\alpha} \mathcal{J}_{\mathrm{M}}.$$

This is the Machian DoF split: the same source drives both sectors, but only the transverse sector carries admissibility entropy cost and produces inertial resistance to shear-like changes.

To connect with an effective acceleration of the schematic form

$$a_{\mathrm{eff}}(r) = A_0 \left(\frac{r}{r_c}\right)^{1/2},$$

identify a_{eff} as the magnitude of transverse relocking drift required to maintain admissibility when transport is corridor-limited. Introduce a transverse relocking coordinate ϕ with stiffness set by transverse curvature invariants,

$$K_{\perp}(r) \equiv K_0 \mathcal{F}\left(\mathcal{I}\left(H^{\perp}(r)\right)\right).$$

If admissibility narrowing produces

$$K_{\perp}(r) \propto A_0^2 \frac{r}{r_c},$$

then an overdamped relocking law

$$\Gamma_{\phi} \dot{\phi} + K_{\perp}(r) \phi = \mathrm{noise}$$

implies an rms relocking rate

$$a_{\mathrm{eff}}(r) \propto \sqrt{K_{\perp}(r)} \propto A_0 \left(\frac{r}{r_c}\right)^{1/2}.$$

Thus the square-root law in CFT is a stiffness-root law in the transverse admissibility sector, not a modification of GR nor an assumed MOND axiom. The constant A_0 is the vacuum-induced ordering-gradient scale setting transverse stiff-

ness, while r_c is the corridor scale fixed by global Mach sourcing through $\mathcal{J}_M$.

In summary, the Machian DoF split is enforced by the existence of a timelike ordering gradient and its projector algebra. The split is dynamical because the T equation is sourced by a nonlocal Mach functional selecting admissible corridors. Admissibility assigns low entropy cost to longitudinal streaming and high cost to transverse shear through invariants of $H^{\perp}$. An effective square-root acceleration law follows when transverse stiffness grows linearly with radius, yielding $a_{\text{eff}} \propto \sqrt{K_{\perp}}$.

20. Finite Machian Ordering Propagation and Longitudinal Corridor Dynamics

Chronoscalar Field Theory does not allow instantaneous reconfiguration of systems or the propagation of influence as motion through spacetime. Instead, the system evolves through admissible ordering configurations defined by the scalar field $T\left(x^{\mu}\right)$, progressing along finite-support corridors. These corridors are shaped by local admissibility and global Machian sourcing. This section clarifies how Machian influence propagates rapidly but finitely, and why this is neither relativistic transport nor quantum entanglement.

The central object is the longitudinal ordering direction $n^{\mu} = \nabla^{\mu} T / \sqrt{-\nabla T \cdot \nabla T}$. Variations along n^{μ} incur minimal admissibility cost, while transverse variations produce entropy via invariants of the transverse Hessian $H^{\perp}_{\mu\nu}$. Consequently, evolution following a disturbance preferentially relaxes along integral curves of n^{μ}, termed Machian ordering corridors. These corridors are global structures in ordering space, not spacetime, dictating how systems reconfigure after an event.

Crucially, ordering propagation does not correspond to the transport of matter, energy, or information at some velocity. There is no signal front or causal cone. Instead, admissible histories are continuous mappings $\gamma : \lambda \mapsto x^{\mu}(\lambda)$, where $T\left(\gamma(\lambda)\right)$ increases monotonically with finite support width. The parameter λ labels ordering progression, not physical time. Finite support requires a nonzero ordering relaxation scale τ_T, such that

$$\Delta T \sim \left|\frac{\mathrm{d}T}{\mathrm{d}\lambda}\right| \tau_T, \quad \tau_T > 0,$$

forbidding instantaneous reordering, but allowing rapid global correlation once a corridor is established. This is the precise sense in which Machian response is fast but not instantaneous.

The corridor structure originates from the global Mach functional $\mathcal{J}_{\mathrm{M}}[T;\rho]$, which depends on the integrated matter distribution. The admissible ordering corridors are globally correlated even before local disturbances. When an event induces strong transverse curvature—such as fracture or discharge—the system cannot relax isotropically. Instead, transverse admissibility collapses locally, forcing the system to relax along the pre-existing longitudinal corridor. The apparent

immediacy of distant responses arises from synchronized relocking, not propagation.

A concrete example is high-field electrical discharge. Measurements show that large-scale electric field reconfiguration following an initial breakdown occurs on timescales much shorter than expected from diffusive charge transport alone, without evidence of superluminal signaling. In CFT, the breakdown produces a sharp increase in transverse ordering curvature. The system's admissible response redistributes ordering along the longitudinal corridor defined by the global electric and mass distribution. Subsequent streamer development follows this corridor, minimizing transverse admissibility cost and explaining the observed continuity of discharge paths without invoking instantaneous action or quantum entanglement.

This same corridor logic applies to mechanical fracture and seismic slip. Laboratory and geophysical observations show that stress redistribution after rupture can appear simultaneous over extended regions, despite finite wave speeds. Within CFT, rupture corresponds to a local collapse of transverse admissibility. The system then relaxes by reordering along longitudinal corridors determined by the global stress and mass distribution, leading to rapid relocking of distant regions into a new admissible configuration.

Mathematically, this can be characterized by an ordering slope invariant

$$\chi \equiv \frac{\sqrt{-\nabla_\mu T \nabla^\mu T}}{\sqrt{\mathcal{I}\left(H^\perp\right)}},$$

where $\mathcal{I}\left(H^\perp\right)$ is a positive transverse curvature invariant. Admissibility requires $0 < \chi < \chi_{\max}$, with $\chi_{\max}$ set by vacuum stiffness and Machian sourcing. This bound replaces relativistic velocity limits in CFT, constraining the rate of admissible reordering rather than motion through spacetime. Systems respond as rapidly as allowed by $\chi_{\max}$, which can be much larger than macroscopic transport speeds while remaining finite and non-instantaneous.

It is important to distinguish this from quantum entanglement. In entanglement, correlations are encoded in a nonlocal wavefunction. In CFT, correlations arise because the ordering corridor exists as a consequence of global matter sourcing. A local event does not transmit correlation; it selects among admissible configurations constrained by the Machian functional. The resulting behavior may appear coordinated over large distances, but it does not involve nonlocal state collapse or violation of finite-support evolution.

This corridor logic applies across scales. In condensed-matter systems, rapid phase relocking following quenches or perturbations occurs along low-entropy ordering directions defined by lattice and electronic structure, as seen in ultrafast superconducting and charge-density-wave experiments. In astrophysical systems, structural reconfiguration following mergers or collapses proceeds preferentially along filaments and planes defined by the global mass distribution, consistent with corridor-limited ordering rather than isotropic relaxation. The rapidity of these

responses reflects low transverse admissibility cost, not infinite propagation speed.

In summary, Machian ordering propagation in CFT is neither spacetime motion nor instantaneous influence. It is finite, corridor-limited reordering along longitudinal directions selected by global matter sourcing. The admissibility framework enforces continuity, finite support, and entropy constraints, while allowing rapid global coordination without invoking relativistic transport, quantum entanglement, or metric dynamics. This defines the physical meaning of Machian corridors as paths of least ordering resistance, setting the stage for discussions of exclusion, holonomy, and boundary-locked admissibility phenomena.

21. Conclusions

This work has established Chronoscalar Field Theory as a self-contained framework in which time is treated as a physical ordering scalar rather than as a passive parameter or coordinate label. From this starting point, the theory derives—rather than assumes—the existence of a Machian degrees-of-freedom split, finite-support admissibility, and a hierarchy of ordering responses that span atomic, condensed-matter, and astrophysical systems. At no stage is Riemannian geometry, spacetime curvature dynamics, or instantaneous influence invoked. The metric enters only as a kinematic bilinear for projection and bookkeeping, not as a dynamical object.

The Machian degrees-of-freedom split was shown to arise unavoidably from the existence of a timelike ordering gradient. Longitudinal variations along this gradient correspond to low-entropy streaming with minimal admissibility cost, while transverse variations correspond to shear, curvature microstructure, and entropy production. This split is mathematically enforced by projector algebra and the structure of the ordering Hessian, and it governs how systems resist, relax, and reorganize following perturbation. Inertia, within this framework, is not a fundamental property but an emergent resistance associated with transverse admissibility costs imposed by global matter sourcing.

Finite-support admissibility plays a central role throughout. By forbidding infinitesimal ordering histories and enforcing nonnegative ordering entropy production, the theory excludes instantaneous reconfiguration while allowing rapid global coordination. Apparent near-simultaneity in physical systems—ranging from lightning initiation and fracture dynamics to phase relocking and large-scale structure formation—is reinterpreted as relocking along pre-existing Machian ordering corridors. Nothing propagates through spacetime at superluminal speed; rather, systems reconfigure along corridors already selected by the global ordering field.

The theory further demonstrates that several phenomena traditionally treated as conceptually distinct—atomic orbital structure, NMR and ESR relaxation, Josephson phase coherence, Meissner exclusion, Aharonov-Bohm holonomy, Berry phase accumulation, and boundary-locked transport in topological materials—

are unified as different diagnostics of the same underlying ordering manifold. Static imaging modes probe admissible geometry, relaxation experiments probe local relocking stiffness, exclusion phenomena probe transverse admissibility collapse, and holonomy phenomena probe global corridor consistency. In each case, the observed behavior follows directly from admissibility constraints and the Machian sourcing of the ordering field.

Importantly, the framework produces concrete, testable scaling laws. The square-root acceleration behavior derived from transverse stiffness scaling is shown to arise as a stiffness-root law, not as a modification of Newtonian dynamics or a relativistic correction. The same formalism predicts specific dependencies of relaxation times, critical currents, coherence lengths, and anisotropy responses on curvature invariants and corridor structure. These predictions are quantitative and falsifiable, and they connect directly to existing experimental literature across multiple domains.

In summary, Chronoscalar Field Theory provides a consistent redefinition of relativity in which ordering, not spacetime geometry, is fundamental. General Relativity emerges as a coarse, symmetric limit of a deeper asymmetric ordering theory, valid when admissibility costs are isotropic and longitudinal dominance masks transverse structure. By restoring time asymmetry, finite support, and Machian global sourcing at the foundational level, CFT resolves longstanding conceptual tensions between inertia, causality, and coordination without introducing new forces, hidden variables, or nonphysical mechanisms. The theory therefore offers a coherent path forward for unifying microscopic ordering, macroscopic dynamics, and cosmological structure within a single admissibility-governed framework [83].

Conflicts of Interest

The author declares no conflicts of interest regarding the publication of this paper.

References

[1] Grant, C.A. (2026) From Brownian Motion to Black Holes: Chronoscalar Transport via the Hessian Flip. *International Journal of Quantum Foundations*, **12**, 497-589.

[2] Mach, E. (1893) The Science of Mechanics: A Critical and Historical Account of Its Development. Translated by T. J. McCormack, Open Court.

[3] Jackson, J.D. (1998) Classical Electrodynamics. 3rd Edition, Wiley.

[4] Dirac, P.A.M. (1958) The Principles of Quantum Mechanics. 4th Edition, Oxford University Press.

[5] Schrödinger, E. (1926) Quantisierung als eigenwertproblem. *Annalen der Physik*, **384**, 361-376. https://doi.org/10.1002/andp.19263840404

[6] von Neumann, J. (1955) Mathematical Foundations of Quantum Mechanics. Princeton University Press.

[7] Riess, A.G., Filippenko, A.V., Challis, P., Clocchiatti, A., Diercks, A., Garnavich, P.M., *et al.* (1998) Observational Evidence from Supernovae for an Accelerating Universe and a Cosmological Constant. *The Astronomical Journal*, **116**, 1009-1038.

https://doi.org/10.1086/300499

[8] Landau, L.D. and Lifshitz, E.M. (1977) Quantum Mechanics: Non-Relativistic Theory. 3rd Edition, Pergamon Press.

[9] Einstein, A. (1987-1995) The Collected Papers of Albert Einstein, Vols. 1-4. Princeton University Press.

[10] Bertone, G., Hooper, D. and Silk, J. (2005) Particle Dark Matter: Evidence, Candidates and Constraints. *Physics Reports*, **405**, 279-390. https://doi.org/10.1016/j.physrep.2004.08.031

[11] Berry, M.V. (1984) Quantal Phase Factors Accompanying Adiabatic Changes. *Proceedings of the Royal Society of London. A. Mathematical and Physical Sciences*, **392**, 45-57. https://doi.org/10.1098/rspa.1984.0023

[12] Eremeev, S.V., Landolt, G., Menshchikova, T.V., Slomski, B., Koroteev, Y.M., Aliev, Z.S., *et al.* (2012) Atom-Specific Spin Mapping and Buried Topological States in a Homologous Series of Topological Insulators. *Nature Communications*, **3**, Article No. 635. https://doi.org/10.1038/ncomms1638

[13] Varykhalov, A., Sánchez-Barriga, J., Shikin, A.M., Biswas, C., Vescovo, E., Rybkin, A., *et al.* (2008) Electronic and Magnetic Properties of Quasifreestanding Graphene on Ni. *Physical Review Letters*, **101**, Article No. 157601. https://doi.org/10.1103/physrevlett.101.157601

[14] Purcell, E.M., Torrey, H.C. and Pound, R.V. (1946) Resonance Absorption by Nuclear Magnetic Moments in a Solid. *Physical Review*, **69**, 37-38. https://doi.org/10.1103/physrev.69.37

[15] Bloch, F., Hansen, W.W. and Packard, M. (1946) Nuclear Induction. *Physical Review*, **69**, 127-127. https://doi.org/10.1103/physrev.69.127

[16] Abragam, A. (1961) The Principles of Nuclear Magnetism. Oxford University Press.

[17] Slichter, C.P. (1990) Principles of Magnetic Resonance. 3rd Edition, Springer.

[18] Ernst, R.R., Bodenhausen, G. and Wokaun, A. (1987) Principles of Nuclear Magnetic Resonance in One and Two Dimensions. Oxford University Press.

[19] Mehring, M. (1983) Two-Dimensional NMR Spectroscopy. In: Mehring, M., Ed., *Principles of High Resolution NMR in Solids*, Springer, 186-204. https://doi.org/10.1007/978-3-642-68756-3_5

[20] Redfield, A.G. (1965) The Theory of Relaxation Processes. *Advances in Magnetic and Optical Resonance*, **1**, 1-32. https://doi.org/10.1016/b978-1-4832-3114-3.50007-6

[21] Kubo, R. and Tomita, K. (1954) A General Theory of Magnetic Resonance Absorption. *Journal of the Physical Society of Japan*, **9**, 888-919. https://doi.org/10.1143/jpsj.9.888

[22] Redfield, A.G. (1957) On the Theory of Relaxation Processes. *IBM Journal of Research and Development*, **1**, 19-31. https://doi.org/10.1147/rd.11.0019

[23] Wangsness, R.K. and Bloch, F. (1953) The Dynamical Theory of Nuclear Induction. *Physical Review*, **89**, 728-739. https://doi.org/10.1103/physrev.89.728

[24] Haeberlen, U. (1976) High Resolution NMR in Solids: Selective Averaging. Academic Press.

[25] Solomon, I. (1955) Relaxation Processes in a System of Two Spins. *Physical Review*, **99**, 559-565. https://doi.org/10.1103/physrev.99.559

[26] Tyryshkin, A.M., Tojo, S., Morton, J.J.L., Riemann, H., Abrosimov, N.V., Becker, P., *et al.* (2012) Electron Spin Coherence Exceeding Seconds in High-Purity Silicon. *Nature Materials*, **11**, 143-147. https://doi.org/10.1038/nmat3182

[27] Casimir, H.B.G. and du Pré, F.K. (1938) Note on the Thermodynamic Interpretation of Paramagnetic Relaxation Phenomena. *Physica*, **5**, 507-511. https://doi.org/10.1016/s0031-8914(38)80164-6

[28] Korringa, J. (1950) Nuclear Magnetic Relaxation and Resonnance Line Shift in Metals. *Physica*, **16**, 601-610. https://doi.org/10.1016/0031-8914(50)90105-4

[29] Bloembergen, N., Purcell, E.M. and Pound, R.V. (1948) Relaxation Effects in Nuclear Magnetic Resonance Absorption. *Physical Review*, **73**, 679-712. https://doi.org/10.1103/physrev.73.679

[30] Goldman, M. (1988) Quantum Description of High-Resolution NMR in Liquids. Oxford University Press.

[31] Schmidt-Rohr, K. and Spiess, H.W. (1994) Multidimensional Solid-State NMR and Polymers. Academic Press.

[32] Tycko, R., Barrett, S.E., Dabbagh, G., Pfeiffer, L.N. and West, K.W. (1990) Electronic States in Crystalline Silicon Studied by High-Resolution 29Si NMR. *Physical Review Letters*, **64**, 2583-2586.

[33] Poole, C.P. (1983) Electron Spin Resonance. 2nd Edition, Wiley.

[34] Abragam, A. and Bleaney, B. (1970) Electron Paramagnetic Resonance of Transition Ions. Oxford University Press.

[35] Van Vleck, J.H. (1932) The Theory of Electric and Magnetic Susceptibilities. Oxford University Press.

[36] Hoesch, M., Muntwiler, M., Petrov, V.N., Hengsberger, M., Patthey, L., Shi, M., *et al.* (2004) Spin Structure of the Shockley Surface State on Au(111). *Physical Review B*, **69**, Article 241401. https://doi.org/10.1103/physrevb.69.241401

[37] Kubo, R. (1966) The Fluctuation-Dissipation Theorem. *Reports on Progress in Physics*, **29**, 255-284. https://doi.org/10.1088/0034-4885/29/1/306

[38] LaShell, S., McDougall, B.A. and Jensen, E. (1996) Spin Splitting of an Au(111) Surface State Band Observed with Angle Resolved Photoelectron Spectroscopy. *Physical Review Letters*, **77**, 3419-3422. https://doi.org/10.1103/physrevlett.77.3419

[39] Simon, B. (1983) Holonomy, the Quantum Adiabatic Theorem, and Berry's Phase. *Physical Review Letters*, **51**, 2167-2170. https://doi.org/10.1103/physrevlett.51.2167

[40] Nagaosa, N., Sinova, J., Onoda, S., MacDonald, A.H. and Ong, N.P. (2010) Anomalous Hall Effect. *Reviews of Modern Physics*, **82**, 1539-1592. https://doi.org/10.1103/revmodphys.82.1539

[41] Koroteev, Y.M., Bihlmayer, G., Gayone, J.E., Chulkov, E.V., Blügel, S., Echenique, P.M., *et al.* (2004) Strong Spin-Orbit Splitting on Bi Surfaces. *Physical Review Letters*, **93**, Article 046403. https://doi.org/10.1103/physrevlett.93.046403

[42] Xiao, D., Chang, M. and Niu, Q. (2010) Berry Phase Effects on Electronic Properties. *Reviews of Modern Physics*, **82**, 1959-2007. https://doi.org/10.1103/revmodphys.82.1959

[43] Josephson, B.D. (1962) Possible New Effects in Superconductive Tunnelling. *Physics Letters*, **1**, 251-253. https://doi.org/10.1016/0031-9163(62)91369-0

[44] Stewart, W.C. (1968) Current-Voltage Characteristics of Josephson Junctions. *Applied Physics Letters*, **12**, 277-280. https://doi.org/10.1063/1.1651991

[45] McCumber, D.E. (1968) Effect of Ac Impedance on Dc Voltage-Current Characteristics of Superconductor Weak-Link Junctions. *Journal of Applied Physics*, **39**, 3113-3118. https://doi.org/10.1063/1.1656743

[46] Barone, A. and Paternò, G. (1982) Physics and Applications of the Josephson Effect. Wiley. https://doi.org/10.1002/352760278x

[47] Tinkham, M. (1996) Introduction to Superconductivity. 2nd Edition, McGraw-Hill.

[48] Van Harlingen, D.J. (1995) Phase-Sensitive Tests of the Symmetry of the Pairing State in the High-Temperature Superconductors—Evidence for $d_{x^2-y^2}$ Symmetry. *Reviews of Modern Physics*, **67**, 515-535. https://doi.org/10.1103/revmodphys.67.515

[49] Aharonov, Y. and Bohm, D. (1959) Significance of Electromagnetic Potentials in the Quantum Theory. *Physical Review*, **115**, 485-491. https://doi.org/10.1103/physrev.115.485

[50] Tsuei, C.C. and Kirtley, J.R. (2000) Pairing Symmetry in Cuprate Superconductors. *Reviews of Modern Physics*, **72**, 969-1016. https://doi.org/10.1103/revmodphys.72.969

[51] Meissner, W. and Ochsenfeld, R. (1933) Ein neuer effekt bei eintritt der supraleitfähigkeit. *Die Naturwissenschaften*, **21**, 787-788. https://doi.org/10.1007/bf01504252

[52] London, F. and London, H. (1935) The Electromagnetic Equations of the Supracoductor. *Proceedings of the Royal Society of London*, *Series A*, **149**, 71-88.

[53] de Gennes, P.G. (1966) Superconductivity of Metals and Alloys. W.A. Benjamin.

[54] Prozorov, R. and Giannetta, R.W. (2006) Magnetic Penetration Depth in Unconventional Superconductors. *Superconductor Science and Technology*, **19**, R41-R67. https://doi.org/10.1088/0953-2048/19/8/r01

[55] Bardeen, J., Cooper, L.N. and Schrieffer, J.R. (1957) Theory of Superconductivity. *Physical Review*, **108**, 1175-1204. https://doi.org/10.1103/physrev.108.1175

[56] Doll, R. and Näbauer, M. (1961) Experimental Proof of Magnetic Flux Quantization in a Superconducting Ring. *Physical Review Letters*, **7**, 51-52. https://doi.org/10.1103/physrevlett.7.51

[57] Basov, D.N. and Timusk, T. (2005) Electrodynamics of High-T_c Superconductors. *Reviews of Modern Physics*, **77**, 721-779. https://doi.org/10.1103/revmodphys.77.721

[58] Hardy, W.N., Bonn, D.A., Morgan, D.C., Liang, R. and Zhang, K. (1993) Precision Measurements of the Temperature Dependence of λ In YBa2Cu3O6.95: Strong Evidence for Nodes in the Gap Function. *Physical Review Letters*, **70**, 3999-4002. https://doi.org/10.1103/physrevlett.70.3999

[59] Clem, J.R. (1969) Penetration Depth and Coherence Length in Superconductors. In: Parks, R.D., Ed., *Superconductivity*, Vol. 1, Marcel Dekker.

[60] Olariu, S. and Popescu, I.I. (1985) The Quantum Effects of Electromagnetic Fluxes. *Reviews of Modern Physics*, **57**, 339-436. https://doi.org/10.1103/revmodphys.57.339

[61] Chambers, R.G. (1960) Shift of an Electron Interference Pattern by Enclosed Magnetic Flux. *Physical Review Letters*, **5**, 3-5. https://doi.org/10.1103/physrevlett.5.3

[62] Peshkin, M. and Tonomura, A. (1989) The Aharonov-Bohm Effect. Springer.

[63] Tonomura, A., Osakabe, N., Matsuda, T., Kawasaki, T., Endo, J., Yano, S., *et al.* (1986) Evidence for Aharonov-Bohm Effect with Magnetic Field Completely Shielded from Electron Wave. *Physical Review Letters*, **56**, 792-795. https://doi.org/10.1103/physrevlett.56.792

[64] Washburn, S. and Webb, R.A. (1986) Aharonov-Bohm Effect in Normal Metal Quantum Coherence and Transport. *Advances in Physics*, **35**, 375-422. https://doi.org/10.1080/00018738600101921

[65] Wilczek, F. and Zee, A. (1984) Appearance of Gauge Structure in Simple Dynamical

Systems. *Physical Review Letters*, **52**, 2111-2114. https://doi.org/10.1103/physrevlett.52.2111

[66] Imry, Y. (2002) Introduction to Mesoscopic Physics. 2nd Edition, Oxford University Press.

[67] Altshuler, B.L., Aronov, A.G. and Khmelnitsky, D.E. (1982) Effects of Electron-Electron Collisions with Small Energy Transfers on Quantum Localisation. *Journal of Physics C*: *Solid State Physics*, **15**, 7367-7386. https://doi.org/10.1088/0022-3719/15/36/018

[68] van Houten, H., C. Beenakker, W.J. and Staring, A.A.M. (1992) Quantum Transport in Semiconductor Nanostructures. In: Grabert, H. and Devoret, M.H., Eds., *Single Charge Tunneling*, Plenum.

[69] Hasan, M.Z. and Kane, C.L. (2010) *Colloquium*: Topological Insulators. *Reviews of Modern Physics*, **82**, 3045-3067. https://doi.org/10.1103/revmodphys.82.3045

[70] Qi, X. and Zhang, S. (2011) Topological Insulators and Superconductors. *Reviews of Modern Physics*, **83**, 1057-1110. https://doi.org/10.1103/revmodphys.83.1057

[71] Xia, Y., Qian, D., Hsieh, D., Wray, L., Pal, A., Lin, H., *et al.* (2009) Observation of a Large-Gap Topological-Insulator Class with a Single Dirac Cone on the Surface. *Nature Physics*, **5**, 398-402. https://doi.org/10.1038/nphys1274

[72] Chen, Y.L., Chu, J.-H., Analytis, J.G., Liu, Z.K., Igarashi, K., Kuo, H., *et al.* (2010) Massive Dirac Fermion on the Surface of a Magnetically Doped Topological Insulator. *Science*, **329**, 659-662. https://doi.org/10.1126/science.1189924

[73] Zhang, H., Liu, C., Qi, X., Dai, X., Fang, Z. and Zhang, S. (2009) Topological Insulators in Bi2Se3, Bi2Te3 and Sb2Te3 with a Single Dirac Cone on the Surface. *Nature Physics*, **5**, 438-442. https://doi.org/10.1038/nphys1270

[74] Dziawa, P., Kowalski, B.J., Dybko, K., Buczko, R., Szczerbakow, A., Szot, M., *et al.* (2012) Topological Crystalline Insulator States in Pb_{1-X} Sn_xSe. *Nature Materials*, **11**, 1023-1027. https://doi.org/10.1038/nmat3449

[75] Wang, J., Lian, B. and Zhang, S.-C. (2014) Quantum Anomalous Hall Effect in Magnetic Topological Insulators. *Physical Review B*, **89**, Article 085106.

[76] Dalibard, J., Gerbier, F., Juzeliūnas, G. and Öhberg, P. (2011) *Colloquium*: Artificial Gauge Potentials for Neutral Atoms. *Reviews of Modern Physics*, **83**, 1523-1543. https://doi.org/10.1103/revmodphys.83.1523

[77] Goldman, N., Juzeliūnas, G., Öhberg, P. and Spielman, I.B. (2014) Light-Induced Gauge Fields for Ultracold Atoms. *Reports on Progress in Physics*, **77**, Article 126401. https://doi.org/10.1088/0034-4885/77/12/126401

[78] Aidelsburger, M., Atala, M., Lohse, M., Barreiro, J.T., Paredes, B. and Bloch, I. (2013) Realization of the Hofstadter Hamiltonian with Ultracold Atoms in Optical Lattices. *Physical Review Letters*, **111**, Article 185301. https://doi.org/10.1103/physrevlett.111.185301

[79] Miyake, H., Siviloglou, G.A., Kennedy, C.J., Burton, W.C. and Ketterle, W. (2013) Realizing the Harper Hamiltonian with Laser-Assisted Tunneling in Optical Lattices. *Physical Review Letters*, **111**, Article 185302. https://doi.org/10.1103/physrevlett.111.185302

[80] Bernevig, B.A., Hughes, T.L. and Zhang, S. (2006) Quantum Spin Hall Effect and Topological Phase Transition in HgTe Quantum Wells. *Science*, **314**, 1757-1761. https://doi.org/10.1126/science.1133734

[81] Fu, L. and Kane, C.L. (2007) Topological Insulators with Inversion Symmetry. *Phys-*

ical Review B, **76**, Article 045302. https://doi.org/10.1103/physrevb.76.045302

[82] Fu, L., Kane, C.L. and Mele, E.J. (2007) Topological Insulators in Three Dimensions. *Physical Review Letters*, **98**, Article 106803. https://doi.org/10.1103/physrevlett.98.106803

[83] Bondi, H. and Samuel, J. (1997) The Lense-Thirring Effect and Mach's Principle. *Physics Letters A*, **228**, 121-126. https://doi.org/10.1016/s0375-9601(97)00117-5

Appendix: Toy Exclusion Law from Admissibility: Why Two Identical Odd-Parity Excitations Cannot Share One Transverse Eigenstate

In CFT, the exclusion rule for identical odd-parity transverse excitations follows directly from admissibility: finite support and nonnegative ordering entropy production. It is not postulated. The purpose of this appendix is to show how admissibility alone enforces exclusion.

Transverse microstructure and orientation index. Let the ordering gradient be timelike,

$$X \equiv -\nabla_\mu T \nabla^\mu T > 0,\ n^\mu \equiv \frac{\nabla^\mu T}{\sqrt{X}},\ P_{\mu\nu} \equiv g_{\mu\nu} + n_\mu n_\nu.$$

The transverse projected Hessian is

$$H^\perp_{\mu\nu} \equiv P_\mu{}^\alpha P_\nu{}^\beta \nabla_\alpha \nabla_\beta T,\ \tilde{H}^\perp_{\mu\nu} \equiv H^\perp_{\mu\nu} - \frac{1}{3}\left(\mathrm{Tr} H^\perp\right) P_{\mu\nu}. \tag{131}$$

Choose a transverse orthonormal triad $\left\{e^a_\mu\right\}_{a=1}^3$ in which $\tilde{H}^\perp$ is diagonal:

$$\tilde{H}^\perp_{\mu\nu} = \sum_{a=1}^3 \lambda_a e^a_\mu e^a_\nu,\ \lambda_1 + \lambda_2 + \lambda_3 = 0. \tag{132}$$

Define the purely geometric orientation index

$$\mathcal{O} \equiv \mathrm{sgn}\left(\det \tilde{H}^\perp\right) = \mathrm{sgn}\left(\lambda_1 \lambda_2 \lambda_3\right) \in \{+1, -1\}. \tag{133}$$

This index records transverse handedness and is odd under reversal of a single eigen-direction. It carries the odd-parity structure without invoking quantum postulates.

Admissibility cost. Admissibility requires finite support along the ordering direction and nonnegative entropy production,

$$\sigma_T = \gamma_1 \tilde{H}^\perp_{\mu\nu} \tilde{H}^{\mu\nu}_\perp + \gamma_2 \left(\mathrm{Tr} H^\perp\right)^2 + \gamma_3 \mathcal{A}\left(\tilde{H}^\perp\right),\ \gamma_i \geq 0. \tag{134}$$

The anisotropy functional $\mathcal{A}$ penalizes rank-reduction cusps: when one eigenvalue is driven toward zero while others remain finite, transverse geometry pinches and entropy cost rises sharply.

Consider a localized transverse excitation of support $\ell_\perp^3$ over corridor thickness ℓ_T,

$$T \mapsto T + \delta T,\ \delta T \approx \psi(x),$$

which shifts the eigenvalues by $\delta\lambda_a$. Admissibility suppresses histories by $\exp\left(-\int \sigma_T \mathrm{d}\tau\right)$; thus σ_T must remain finite.

Two identical odd-parity excitations in one eigen-channel. Let an odd-parity excitation carry definite orientation index $\mathcal{O}$ and be dominated by one eigen-direction, say $a = 1$:

$$\delta \tilde{H}^\perp_{\mu\nu} \approx \delta\lambda_1 e^1_\mu e^1_\nu,\ \delta\lambda_2 \approx \delta\lambda_3 \approx -\frac{1}{2}\delta\lambda_1. \tag{135}$$

Place two identical excitations with the same $\mathcal{O}$ into the same channel. In

their overlap,

$$\delta\lambda_1 \to 2\delta\lambda_1, \tag{136}$$

and the eigenvalue differences double. Anisotropy therefore grows superlinearly and

$$\sigma_T^{\text{overlap}} \gtrsim \gamma_1 \left\| \tilde{H}^{\perp} \right\|^2 \to 4\gamma_1 \left\| \tilde{H}^{\perp} \right\|^2. \tag{137}$$

Because corridor thickness ℓ_T is fixed by admissibility, the system cannot dilute this cost by widening support.

Forced outcomes. Only two responses avoid divergence:

1) Rank-reduction cusp: one eigenvalue is driven toward zero,

$$\exists \text{overlap point(s) with } \lambda_a \to 0, \tag{138}$$

but cusp formation is precisely what $\mathcal{A}\left(\tilde{H}^{\perp}\right)$ penalizes, suppressing such histories.

2) Support collapse: overlap shrinks to zero corridor width, violating finite support.

(**CFT exclusion law**) Two identical odd-parity transverse excitations cannot occupy the same eigenstate of $\tilde{H}^{\perp}$ within one admissible corridor.

Orientation index under superposition. With

$$\tilde{H}^{\perp} = \tilde{H}_0^{\perp} + \delta\tilde{H}_{(1)}^{\perp} + \delta\tilde{H}_{(2)}^{\perp},$$

identical same-channel excitations are co-diagonalizable, so

$$\det\left(\tilde{H}_0^{\perp} + \delta\tilde{H}_{(1)}^{\perp} + \delta\tilde{H}_{(2)}^{\perp}\right) = \prod_{a=1}^{3}\left(\lambda_{0,a} + \delta\lambda_{(1),a} + \delta\lambda_{(2),a}\right),$$

and the orientation index remains coherent, removing any possibility of local sign cancellation and forcing the cusp alternative.

Corridor thickness is not tunable. Corridor thickness ℓ_T emerges from stability of the ordering gradient:

$$X = -\nabla_\mu T \nabla^\mu T > 0, \; n^\mu = \frac{\nabla^\mu T}{\sqrt{X}}, \; n_\mu n^\mu = -1.$$

If support were arbitrarily compressed, fluctuations would drive $X \to 0$ or change its sign, destroying the timelike ordering direction and the 1 + 3 split $\left(n^\mu, P_{\mu\nu}\right)$. Finite ℓ_T is therefore an admissibility requirement of the ordering geometry itself.